NOVA SCHOOL OF SCIENCE & TECHNOLOGY

DEPARTAMENT OF PHYSICS

BIOPRINTING OF ENZYMATICALLY CROSSLINKED HYALURONIC ACID-GELATIN HYDROGELS

TERESA DÍAZ JORDÀ

BSc in Biotechnology

MASTER IN BIOMATERIALS AND NANOMEDICINE

NOVA University Lisbon

September, 2023

DEPARTAMENT OF
PHYSICS

BIOPRINTING OF ENZYMATICALLY CROSSLINKED HYALURONIC ACID-GELATIN HYDROGELS

TERESA DÍAZ JORDÁ

BSc in Biotechnology

Advisor: PhD Full Professor Gloria Gallego Ferrer
Centre for Biomaterials and Tissue Engineering (CBIT)
Universitat Politècnica de València (Spain)

Co-advisors: PhD Principal Researcher Paula Soares
NOVA University Lisbon

MASTER IN BIOMATERIALS AND NANOMEDICINE

NOVA University Lisbon
September, 2023

Bioprinting of Enzymatically Crosslinked Hyaluronic acid-Gelatin Hydrogels

Acknowledgments

First, I would like to acknowledge the financial support from the Generalitat Valenciana through the Consellería de Innovación, Universidades, Ciencia y Sociedad Digital to support this Master Thesis Project. Grant reference was CIPROM/2022/43, entitled "Liver cell models based on decellularized printable hydrogels for high-throughput drug screening" with acronym LIVERGEL.

I would like to thank my co-advisors Prof. Gloria Gallego Ferrer and Julio Rodríguez Fernández for welcoming me in the group and giving me the opportunity to get involved in this exciting project. Thanks as well all the team at CBIT for their support, and all the advice and help during these months. I would like to thank Prof. Paula Soares as well for her support in the distance.

Infinite thanks to my mother and friends, that have been there during all ups and downs during a difficult yet rewarding period.

ABSTRACT

Three-dimensional printing of biological materials is enabling the development of emerging applications of tissue engineering constructs for regenerative and personalized medicine, and engineered tissue models of disease and diagnosis. Hydrogel-based bioinks for extrusion bioprinting are widely applied; however, the development of a new bioink faces the challenge of complying with all printability requirements, as well as having suitable physico-chemical properties to provide cells with a biocompatible microenvironment during and after the printing process. Low shear flow and high shape retention are two key properties for dispensing bioinks. This study introduces the synthesis and characterization of tyramine-grafted hyaluronic acid (HA) and gelatin (Gel) bioinks, with a horseradish peroxidase/hydrogen peroxide enzymatic crosslinking system to trigger in-demand layer-by-layer gelation over an extruded pattern with an additional drop deposition printhead. HA-based inks (1-4% solutions) and their mixtures with Gel (HA-Gel proportion 80/20 v/v) showed a shear-thinning behavior to be extruded properly. Higher concentrations of polymer yielded an improved construct quality. HA-Gel bioinks were printed together with hepatocarcinoma (HepG2) cells using two sizes of nozzle gauge (20G and 22G). Cell viability was not impacted by the different nozzle size applied, whereas polymer concentration showed a significant effect. In this regard, HA-Gel 4% had a post-printing viability around 90%, and HA-Gel 5% was reduced by half to approxximately 45%. Moreover, the assessment of the miscibility of the two bioinks (HA-based and HA-Gel 80/20) provided us with an insight into how much gap shall be considered between contiguous structures to be independent while in contact with each other. For HA-Gel mixtures, a gap of at least 3-4 times the filament width needs to be considered during the design. These bioinks have shown the capability to be extruded, as good quality 3D cell-laden constructs with a biocompatible printing and gelation system, and have the potential to be applied for more complex co-culture models.

Keywords: bioink, gelatin, hyaluronic acid, HepG2, printability

RESUMO

A impressão tridimensional de materiais biológicos está a facilitar o desenvolvimento de aplicações emergentes de engenharia de tecidos como de modelos tisulares de doenças e diagnóstico. As biotintas à base de hidrogel para bioimpressão por extrusão são amplamente aplicadas; no entanto, o desenvolvimento de uma nova biotinta enfrenta o desafio de cumprir todos os requisitos de printabilidade, para além de ter propriedades físico-químicas adequadas para proporcionar às células um microambiente biocompatível durante e após o processo de impressão. Este trabalho apresenta a síntese e a caraterização de biotintas de ácido hialurónico (HA) e gelatina (Gel) com enxerto de tiramina, com um sistema de reticulação enzimática com a enzima HRP (*horseradish peroxidase*) e peróxido de hidrogénio (H_2O_2) para desencadear a gelificação *layer-by-layer* e em demanda sobre um padrão extrudido com um sistema adicional de deposição de gotas. As tintas à base de HA (soluções 1-4%) e as suas misturas com gelatina (HA/Gel 80:20 v/v) apresentaram um comportamento de viscosidade adequado para serem extrudidas. Concentrações mais elevadas de polímero produziram uma melhor qualidade de construção. As biotintas HA-Gel foram impressas juntamente com células de hepatocarcinoma (HepG2) utilizando dois tamanhos de calibre de injetor (20G e 22G). A viabilidade celular não foi afetada pelos diferentes tamanhos de injetor aplicados, enquanto a concentração de polímero mostrou um efeito significativo, onde o HA-Gel 4% teve uma viabilidade pós-impressão de aproximadamente 90%, e o HA-Gel 5% foi reduzido pela metade até 45%. Além disso, a avaliação da miscibilidade proporcionou uma ideia da distância que deve ser considerada entre estruturas contíguas para serem independentes quando em contacto umas com as outras. Para as misturas HA-Gel, é necessário considerar um espaço de pelo menos 3-4 vezes a espessura do filamento durante o desenho. Contudo, estas biotintas demonstraram a capacidade de serem extrudidas como construções 3D carregadas de células de boa qualidade com um sistema de impressão e gelificação biocompatível, e têm o potencial de serem aplicadas em modelos de co-cultura mais complexos.

Palavras chave: biotinta, gelatina, ácido hialurónico, HepG2, printabilidade

CONTENTS

LIST OF FIGURES

LIST OF TABLES

ACRONYMS

CAD	Computer-aided design
Gel	Gelatin
H_2O_2	Hydrogen peroxide
HA	Hyaluronic acid
HMW	High molecular weight
kPa	Kilo-Pascal
LMW	Low molecular weight
Tyr	Tyramine

1

INTRODUCTION

1.1 Bioprinting

Three-dimensional (3D) bioprinting comprises a range of emerging technologies that allow the fabrication of cell-laden structures with a more complex architecture than other scaffolds or cell culture supports traditionally used. First prototyped in the 1980's decade by Charles W. Hull, 3D printing was initially named stereolithography, in which thin layers of material were deposited layer-by-layer and further cured under UV light exposure, ultimately forming a three-dimensional solid structure. This process is now widely applied to manufacture resin molds for scaffolding across several industries. The development of aqueous and biocompatible materials opened the door to the application of 3D printing in the field of tissue engineering, combining advances in cell biology and materials science. In recent years it has become a versatile technology with the potential to produce biological constructs, such as bone scaffolds, organ-on-chip platforms, or organoids (Chliara et al., 2022; Datta et al., 2020; Tang et al., 2016). The simultaneous incorporation of cells with a biomaterial has the potential to allow the proliferation of cells in a designed structure. Hence, animal-free *in vitro* platforms for drug toxicity screening or potential tissue replacement approaches are fields in which bioprinting is gaining popularity. Overall, 3D bioprinting comprises a set of additive manufacturing techniques where a pattern of biological material is deposited onto a substrate. There exist, however, novel strategies such as tomographic printing that operate under a different principle and are beyond the scope of this study.

Three main strategies for 3D bioprinting can be distinguished: inkjet, laser-assisted, and extrusion-based printing. The common component to all three is the bioink, while each

strategy differs in its deposition system, speed, or resolution, and has its own properties and limitations. (Moroni et al., 2018)

Inkjet bioprinting consists of the controlled deposition by drops of a bioink volume onto a surface, usually through piezoelectric, thermal, or electromagnetic valves to eject the drops from the cartridge. Nevertheless, the inks used must be rather liquid since it is susceptible to clogging of the nozzle (ca. 50 μm diameter), which can be a limitation when a solid and uniform 3D structure is desired upon deposition. Overall, it remains a fast and relatively cheap technique. Despite having been used in the area of tissue engineering, the cell densities achieved are generally low,.(Li et al., 2020; Murphy & Atala, 2014) since cells can hardly be homogeneously suspended in a low-viscosity bioink as required. It has been applied to produce cell-laden cartilage implants (Cui et al., 2012) or liver cell culture models (Arai et al., 2017; Parsa et al., 2010) , however, its most wide application in this area is the fabrication of organ-on-chip platforms, combined with other technologies such as microfluidics. (Moya et al., 2018)

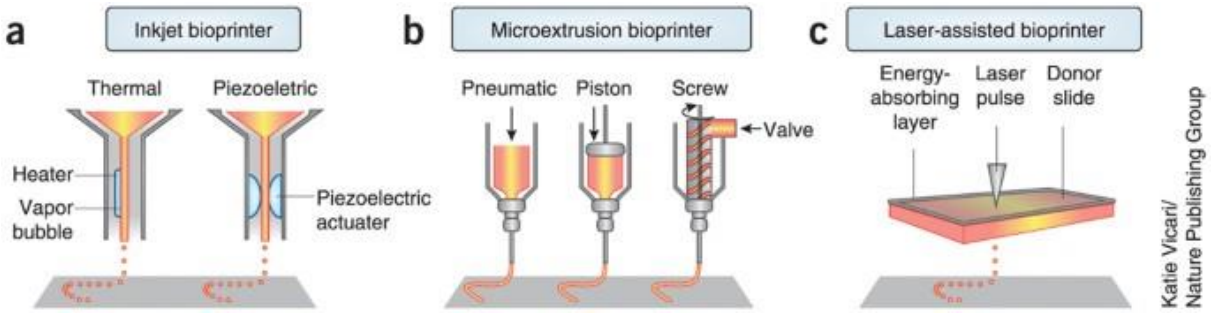

Figure 1.1 Components of inkjet (A), microextrusion (B) and laser-assisted bioprinters (C). (A) Inkjet allows the controlled deposition of drops by means of thermal or piezoelectric opening valves. (B) Microextrusion allows the deposition of a filament by pneumatic pressure or mechanical valves (piston or screw). (C) Laser-induced formation of drops on a bioink by localized bubble formation via an energy absorbing layer. (Murphy & Atala, 2014)

Laser-assisted bioprinting allows high-velocity (10 m/s) deposition of cell solutions with high cell concentrations. A donor surface with a light-absorbing layer on top of a bioink layer, a substrate, and a pulsed laser source are the typical components of a laser-assisted bioprinting system. When exposed to light, the light-absorbing layer locally absorbs it, causing it to vaporize and create a strong gas pressure that induces the ejection of droplets of bioink toward the substrate. The complexity of this mechanism is influenced by the amount of light, the length of the laser pulse, the size of the laser spot, the separation between the absorbing layer and the substrate, and the thickness of the bioink layer. Using this method, bioink droplets may be printed with high resolution and good cell viability. (Murphy & Atala, 2014) Cells, however, can be negatively impacted by the laser's heat, and its numerous parameters make it more difficult to tune and set up while requiring bigger volumes of bioink. Additionally,

this equipment has a higher cost than other bioprinting methods. There exist other types of light-assisted technologies that evolve from stereolithography techniques, such as digital light processing (DLP), in which a specific wavelength is projected as a planar pattern and along the z-axis towards a bioink bed, activating photopolymerization. Similar to laser-assisted bioprinting, these techniques compromise cell viability via phototoxicity. (Williams et al., 2005)

Figure 1.2. Cellink BIOX extrusion-based printer. Composed by three printheads with temperature control, laminar flow and console. The printheads move in the X-Y plane while the print bed has a Z axis movement.

Generally, the most widely used as well as affordable type of bioprinters relies on bioink extrusion (or microextrusion). These usually consist of a dispensing system over a printing bed, with either one or both components capable of moving in the x, y, and z axes. The dispensing system may have one or more printheads, in which the bioink-containing cartridges are placed (Figure 1.2). Several printheads allow the deposition of several bioinks, with varying compositions or cell types. Oftentimes, these printers allow the temperature control of both the printhead and the print bed, as it may be desired to keep cell-laden inks at physiological temperature or prevent a certain polymer from reaching its crystallization temperature. Compared to other strategies, extrusion printing performs well with a wide range of viscosities (30 mPa·s to 60 kPa·s). (Gillispie et al., 2020; Murphy & Atala, 2014). The extrusion can be actuated pneumatic or mechanically (screw or piston) (Figure 1.1.B). In general, mechanical systems are more suitable for highly viscous inks, but incorporate smaller and more complex components. In contrast, pneumatically driven systems can be suitable for a wider range of viscosities, despite being limited to the pressure capacity of the pump. The cartridge is coupled to a tip or nozzle, with a cone-like or needle form, with varying gauges. There is a close relationship between

bioink viscosity, extrusion pressure, and nozzle gauge, which will be discussed in the following sections. Moreover, using microextrusion higher cell densities can be achieved, ranging from 1 to 40 million cells per milliliter. (Gillispie et al., 2020)

1.2 Design and processing

Computer-aided design (CAD) is the starting point to define the desired architecture of a bioprinted construct. CAD software is often a user-friendly visual platform that allows you to design the model as a solid, since it is not expected to design the model by layers. The output of this software is an *STL* file that has to be processed to become readable by the printer. Thus, this three-dimensional solid file has to be run through a *slicer* software, that layers the model given some desired parameters (e.g., filament width, layer thickness), and provides the ultimate instructions for the printer. These instructions are given in the form of a text file, written as G-code, which is the programming language understood by 3D printers. The G-code may contain different sorts of commands, from coordinates to extrusion speed, and despite not being immediately intelligible, sometimes researchers might need to manually program specific commands, such as well-to-well transitions. Nevertheless, as more bioprinters become available and the technology rapidly evolves, some of these steps are compiled in open-source tools. (Bonatti et al., 2021; Dávila et al., 2022) While printer manufacturers implement and simplify the printer software and user interface, enabling modification of parameters even during the printing process and allowing researchers to test and optimize printing parameters in dynamic conditions. (Nazir et al., 2023)

1.3 Bioinks

In the context of bioprinting, oftentimes we can find the term bioink indistinctly referring to cell-free inks containing biologically derived or just biocompatible materials, or cell-laden inks. Nevertheless, both kinds need to fulfill the same printability requirements, while cell-laden bioinks need extra considerations (e.g., physiological conditions). For ease of reading, throughout this section, bioinks will always refer to cell-laden inks.

Bioinks are mainly aqueous hydrogel precursor solutions, in which cells can be found dispersed in suspension. To ensure cell viability and survival through the printing process, the solution needs to have a low-elastic modulus but be viscous enough to prevent cells from concentrating at the bottom of the cartridge. Several natural and synthetic polymers have been applied to develop bioinks. Polymers present in the extracellular matrix (ECM) are particularly suitable since they are inherently biocompatible and can have biological activity. These

include native collagen, hydrolyzed collagen (gelatin), fibrin, and hyaluronic acid (Bomo et al., 2016; Hiller et al., 2018; Potere et al., 2022; Schwab et al., 2020). Other non-ECM natural polymers such as alginate (Chang et al., 2008; Ouyang et al., 2016), silk fibroin (Janani et al., 2022), or chitosan (Lazaridou et al., 2022) have been applied to the formulation of bioinks. A wide range of synthetic polymers are also used for hydrogel preparation due to improved mechanical properties, as for example, polyethylene glycol (PEG), or poloxamer (Ribeiro et al., 2018; Rutz et al., 2015). However, these materials lack bioactive sites that promote cell adhesion and migration, unlike ECM-derived polymers.

1.3.1 Bioink crosslinking and construct stability

A challenge to consider in bioink development is the post-printing stability, which would require the hydrogel network to hold its structure and not collapse upon sequential deposition of layers. Mechanically stable constructs rely on the bioink composition and properties, and on whether there is an additional crosslinking step to intertwine the polymer networks. Both strategies are considered altogether, since mechanically stable bioinks are required for the optimal deposition of layer over layer, while crosslinking may be added as an intercalated step (i.e., by layers), or once the construct is fully printed.

In terms of structure, hydrogels are tridimensional networks highly hydrophilic, in which the crosslinking degree modulates the hydration capacity. The crosslinking must establish interactions strong enough to provide stability to the formed hydrogel, while also allowing the diffusion of gas and biomolecules when cells are embedded within the network. Crosslinking may be performed before the bioprinting, to enhance the viscosity of the bioink and improve its printability (Hiller et al., 2018). This previous crosslinking may however not be stable throughout the extrusion process, and subsequent crosslinking is required to improve the stability of the printed construct. Crosslinking during and after the printing process are commonly used strategies. The vast majority of bioprinting studies use methacrylate derivatives of biocompatible polymers, such as gelatin or hyaluronic acid, and rely on photo-catalyzed crosslinking, by introducing a photoinitiator and exposing the blend to UV light of a certain wavelength. (Skardal et al., 2010) The crosslinking degree and as a consequence the mechanical properties of the hydrogel result from the exposure time and intensity of the light. While this might be a suitable approach for cell-laden constructs, a finer tuning of the stiffness of the printed construct may produce DNA damage in the cells due to longer UV exposure and high intensities. (Adhikari et al., 2021)

Reversible physical forces are also used as a form to crosslink the hydrogel networks, by hydrogen bonds, ionic, and van der Waals interactions. Non-covalent bonds do not require any additional crosslinking agents, reducing the risk of side toxicity due to chemical catalyzers or photoinitiators. These bonds might result from hydrophilic-hydrophobic interaction promoting self-assembly of the polymer chains, temperature-driven gelation, opposite chirality, or ionic interactions of polyelectrolytes. While these methods are widely used for drug-delivery devices, in which the dis-entanglement of the matrix is desired under certain conditions (e.g., stomachal acidic environment), their application for long-lasting mechanically stable tissue engineering platforms is limited.(Lazaridou et al., 2022)

Enzymatically crosslinked hydrogels result from enzyme-catalyzed reactions that yield stable covalent bonds. The main advantage of these reactions is that the catalyzers added to the bioink mixture are found in humans, and react under physiological conditions, improving the overall biocompatibility of the crosslinking.(Naranjo-Alcazar et al., 2023)

Depending on the type of molecules used for the bioink, whether they are natural polysaccharide chains, proteins, or synthetic polymers, it will be necessary that the compounds to crosslink have receptor and donor functional groups to form the bond. For example, transglutaminases form bonds between glutamine and lysine residues, thus proteins such as collagen or its hydrolyzed form (i.e. gelatin) may be subject to this crosslinking. (Zhou et al., 2019) Polymer modifications are a common strategy to provide effective sites for crosslinking with a specific enzyme. Yet the applicability of most enzymatic crosslinking systems has been constrained by the poor mechanical characteristics and slow gelation rates. In contrast, the use of horseradish peroxidase (HRP) together with hydrogen peroxide (H_2O_2) provides a fast gelation (seconds), thus allowing a better control over the hydrogel formation. (Bae et al., 2015) HRP catalyzes the crosslinking of phenolic hydroxyl groups forming C-C or C-O bonds, using phenol as a reducing substrate and consuming H_2O_2. Phenolic groups can be chemically conjugated to the main polymer chains, to provide these bonding sites. Tyramine is a common molecule used to introduce phenolic groups and allow the crosslinking between tyramine-grafted polymers. (Petta et al., 2018; Poveda-Reyes et al., 2016; Sanmartín-Masiá et al., 2017)

It is possible to find combined crosslinking strategies, where an initial crosslinking is performed on the precursor to enhance the viscosity, and another strategy is used during and after the printing process. (Hiller et al., 2018; Zhou et al., 2019) For instance, Petta *et al*. have applied a double gelation strategy by first enzymatically crosslinking the tyramine-hyaluronic acid (HA-Tyr) inks to be printed, followed by UV photopolymerization. (Petta et al., 2018)

When considering a crosslinking method that requires the addition of another agent like an enzyme to the polymer mixture, there are several ways to put both phases in contact.

It is common to either print directly onto an aqueous bath containing the crosslinking agent, or to immerse the fully printed construct in such solution after printing. (Hiller et al., 2018; Sakai et al., 2021) Sakai *et al.* showed a cascade enzymatic mechanism in which HRP coupled with a reaction yielding H_2O_2 in the printing bed, to crosslink cell-laden HA-based bioinks.

1.3.2 Bioink properties

While the composition of the bioink is key in terms of biocompatibility, the translation of a simple hydrogel cell culture support to a printable bioink requires an evaluation of its mechanical properties, both of precursor hydrogel solutions (e.g., pre-crosslinking) and printed constructs. Properties such as viscosity, elasticity, and surface tension, have a great influence in its ability to flow properly through the dispensing system and deposit precisely and uniformly on the printing bed. These physicochemical factors are commonly understood as rheological characteristics. Rheology is the study of how materials change shape and move when forces are applied. In extrusion-based bioprinting, a bioink that is originally present in a bulk resting state changes form while passing through the nozzle, transitions to a high shear condition, and then eventually achieves a new resting state upon deposition. Viscosity, visco-elastic shear moduli, elastic recovery, and shear stress are the main rheological properties that describe these transitions. (Jungst et al., 2016; Schwab et al., 2020)

Namely, viscosity is a crucial feature, since it should be low enough to allow an easy extrusion through the nozzle, while maintaining enough viscosity to hold its structure post-printing. Bioink viscosities in microextrusion-based bioprinting range from 30 mPa·s to 60 kPa·s. Viscosity, which is a fluid's resistance to flowing while under stress, has a significant impact on the print accuracy and effectiveness of cell encapsulation. Enhanced viscosity typically leads to improved printing quality. High viscosity, however, also causes more shear stress, which can have an impact on the cells suspended in the bioink. (Ouyang et al., 2016) The molecular weight and concentration of polymers in solution are the key determinants of their viscosity. (Boularaoui et al., 2020) The shear stress (Pa) to shear rate ratio (s^{-1}) is used to define viscosity (Pa s). Newtonian fluids are defined as having a linear connection between shear stress and shear rate. Non-Newtonian fluids are those that deviate from linearity and have ratios that are either dropping or rising. When this relationship is time-independent, two opposite behaviors can be observed: shear-thinning or shear-thickening. The most common behavior is shear-thinning, in which increasing shear rates decrease its viscosity. This is the ideal behavior for materials to be extruded, since the opposite reaction (shear-thickening),

would make it more difficult to dispense as the viscosity would be higher under higher pressures or forces. Therefore, in extrusion printing of a shear-thinning material, we can expect a decrease of the viscosity during the extrusion phase. Ideally, when the shear rate drops to zero, the extruded ink recovers the initial viscosity, in order to better preserve the printed construct. The initial viscosity is often referred to as **zero-shear viscosity**. Shear thinning is illustrated in figure 1.3 through the nozzle and its behavior observed as a function of shear stress/shear rate. The laminar flow results from the pressure applied, while the shear stress is caused by the friction with the walls of the cartridge and nozzle. The desired response to this shear stress is a shear-thinning behavior, where polymer chains disentangle and orientate along the flow direction, which in turn reduces the viscosity by decreasing the resistance given by intermolecular interactions.

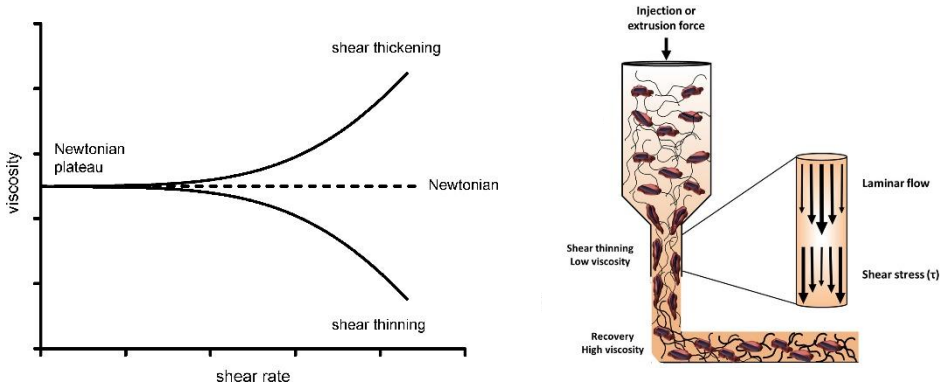

Figure 1.3. Shear thinning behavior of bioinks. Shear thickening and shear thinning behavior represented as a function of viscosity and shear rate (left), from Jungst et al. (2016). Illustrated bioink extrusion with shear thinning behavior (right). Modified from Chopin-Doroteo et al. (2021)

.

Once deposited, the shear stress drops, and the viscosity is expected to increase again. While recovery of the initial viscosity is not guaranteed, the solution extruded was a precursor hydrogel that can then be subject to crosslinking, that would enhance the mechanical properties of the printed construct.

Viscoelasticity is another important property for the printed construct, which is its ability to maintain the integrity and recover its elasticity upon deformation (i.e., extrusion through nozzle). Viscoelastic properties can be determined with oscillatory rheology, while viscosity measurements are done under rotation. In the literature, it is common to find bioink characterization including either viscosity measurements or viscoelasticity (Schwab et al., 2020) . The latter is defined by two parameters: storage modulus (G'), and loss modulus (G''), which can be associated with the elastic energy stored during deformation i.e. extrusion, and the amount of energy dissipated linked to the viscous flow, respectively. The viscoelasticity of the ink as precursor is thus related to the quality of the final construct. On the other end, viscoelasticity

of the complete printed constructs (e.g., after crosslinking, incubation, cell seeding) is often used as part of the mechanical characterization. An adequate surface tension is also key to allow proper adhesion of the bioink to the substrate (e.g., glass plate) and adhesion among layers.

For extrusion-based printing, hydrogel precursors that can be extruded via a thin nozzle and later produce shape-stable gels are appropriate. On one hand, its mechanical properties will determine the dispensing pressure and likely the type of nozzle and gauge at which such ink can be extruded. Both the pressure and indirect stresses from the tip or nozzle can have an impact on cell survival during printing. (Chang et al., 2008) Depending on the sensitivity of different types of cells, higher pressures that cause more shear stress, can reach up to a 100% cell damage. (Boularaoui et al., 2020) Previous studies have proposed models to establish a pressure-cell damage relationship, based on experimental results. (Nair et al., 2009; Ning et al., 2018) . The pressures cells can tolerate are often considered within the range of 30 to 250 kPa in extrusion printing.

The geometry of the nozzle has also shown to have an impact in cell viability, where conical tips appear to yield 10-fold increased cell viability compared to straight cylindrical nozzles. Nozzle diameter can still negatively contribute to cell survival, since smaller diameters have shown to yield to cause more shear stress on cells (Billiet et al., 2014; W. Liu et al., 2017). However, it has also been shown that conical tips can have a more variable flow rate, compromising not only the reproducibility, but also the effect of varying flow rates on cells viability. Thus, using a cylindrical nozzle can be beneficial, while optimizing the tip diameter may be a more important factor affecting cell viability. (Morata Martínez, 2021)

Lastly, the high viscosities of the bioink, and the extrusion pressure and shear stress subsequently, can vary with temperature. Temperature-sensitive gelation, as often used for gelatin-based hydrogels, is also dependent on the holding temperature and temperature change upon deposition. On one hand, increasing printing temperature can be used to decrease fluid viscosity. On the other hand, decreasing temperature might be used to avoid cell sedimentation in low viscosity bioinks. Zhao *et al.* assessed the effect of both printing temperature and holding time (i.e., cells dispersed in bioink prior to printing) in gelatin/alginate-based bioinks. They found that a low temperature like 10˚C has a significantly detrimental effect on cell viability regardless on the holding time, while long holding times (ca. 30 minutes) had a negative impact at any holding temperature from 10 to 20˚C. (Zhao et al., 2015).

1.4 Printability

A proper gelation mechanism, homogeneity of the materials in terms of cell (or if any other fiber or particle component) distribution, cytocompatibility, and swelling/degradation behavior need to be explored and adjusted during the creation of a hydrogel as a bioink. Assessing relevant rheological characteristics of the ink as indicators of the prospective shape fidelity may be the first step in predicting printability before printing. Once this initial assessment has been done, the performance of the bioink in the bioprinter setup needs to be tested and optimized.

Printability comprises a set of parameters that ultimately define the ability to form a 3D structure with fidelity and integrity. The definition might consider different parameters depending on the bioprinting method. For example, inkjet's printability relies on the ability to generate a well-defined droplet with a desired volume, while microextrusion requires the formation of a continuous filament with a controlled diameter. (Kyle et al., 2017; Malekpour & Chen, 2022) Gillispie et al., define printability as "the ability of a material, when subjected to a certain set of printing conditions, to be printed in a way which results in printing outcomes which are desirable for a given application". (Gillispie et al., 2020) Since this framework accepts more parameters as we increase the complexity of the system (e.g., several printheads, multimaterial printing, different cells and composition), every time a variable is modified, such as the polymer concentration, it might be necessary to re-assess the whole workflow and optimize trough an iterative process.

In the context of bioinks for microextrusion, the first printability parameter to consider is extrudability, which is the ability of the bioink to flow, pass through the needle and form a uniform filament, upon application of a certain force or pressure. As it has been noted, viscosity plays a key role in the ability of a bioink to be extruded through a specific nozzle and within the range attainable by the bioprinter. At times, extrudability is defined as the minimum pressure at which the ink can be extruded through the nozzle. (Malekpour & Chen, 2022) The formation of the filament is visually assessed and is directly related to the shear stress-viscosity behavior described previously. The formation of this filament and uniform deposition on a substrate is also dependent on the nozzle offset (Naghieh & Chen, 2021). A relatively big distance between the end of the nozzle and the bed might cause the filament to "curl up" or aggregate within itself. This effect is reduced by reducing the distance between the nozzle and the substrate, but it is susceptible to cause irregularities during the printing process, as layers might partially collapse, and this distance is increased compared to the theoretical height increment. A minor offset, however, may cause the biomaterial to be compressed and inhibit appropriate biomaterial flow during the deposition by clogging the nozzle.

Once the extrudability of a bioink has been confirmed, there are several parameters that can be evaluated in printed constructs, grids, or single lines. Non-dimensional factors such as strand printability, integrity factor, uniformity, or pore factor are all parameters that help us understand the quality of the printed construct and its shape fidelity, compared to the CAD model or an optimal. For instance, uniformity or spreading ratio defines the lateral spreading in width of printed filaments, several layers, compared to perfectly stacked layers with a modelled width. The pore factor, on the other hand, reflects the resolution of the construct considering the inner pore's area, i.e., inner grid squares with a known theoretical area or optimal. (Malekpour & Chen, 2022; Naghieh & Chen, 2021)

Along with these deformations, adjacent filaments printed in the same layer may fuse because of time-dependent flow before stabilization by cross-linking and spread over the underlying layer brought on by surface tension. Printing parallel structures or filaments with a progressive reduction in filament spacing or parallel filaments with a defined gap was suggested as a simple technique to examine such filament fusion. (Ribeiro et al., 2018; Wüst et al., 2014) Altogether, the parameters mainly associated to bioink deformation have been considered in relation to its viscoelastic behavior (Xu et al., 2013) . Thus, a thorough rheological characterization of the bioink might help predict its printing performance and narrow down the number of experiments. (Göhl et al., 2018)

The results of the printability assessment are not only influenced by the bioink itself, but rather of all the printing variables as well as the designed model. Printing speed can have an impact in the printability, since lower viscosities will require higher speeds in order to accelerate the process and avoid strand spreading. However, Naghieh et al. showed that different speeds gave better results for strand uniformity and pore factor separately. Thus, if both parameters are to be considered, then the speed has to be optimized for both and not just one factor. (Naghieh & Chen, 2021) Mathematical models have been proposed to calculate an average extrusion speed. (Paxton et al., 2017)

The quality of the printed constructs might also be affected by the design considered for the assessment. The presence of acute angles can generate the impression of non-suitable or low printability of a construct when it might be solved by finer tuning of the printing parameters or the design itself. Also, when using a design where there are multiple filament intersections (e.g., grid), it is expectable to have accumulated material at these nodes when for one single layer, the dispensing nozzle crosses twice that same point to trace perpendicular filaments. Therefore, the accumulated material produces an accentuated diffusion or spreading of the bioink around these nodes, reducing the perceived quality of the printed construct. (He et al., 2016; Kyle et al., 2017)

While the resolution of the construct might not be as relevant for the simple purpose of automated deposition of a drop-based pattern, it becomes critical to achieve functional biological devices with a precise geometry and compartmentalized distribution.

1.5 Hyaluronic acid and gelatin hydrogels

Hyaluronic acid (HA) is a non-sulfonated glycosaminoglycan present in the extracellular matrix (ECM) in many different tissues across the human body, especially in connective tissues, skin and joint fluids. In the ECM, the interactions of HA with its specific receptor CD44 are associated with fundamental physiological processes, such as embryonic development or pathological conditions in which HA promotes cell proliferation (e.g., tumor microenvironment). Specific isoforms of CD44 receptor are overexpressed by cancer cells, thus the interplay between ECM HA and the receptor has been shown to have a crucial role in tumorigenic signaling pathways. (Misra et al., 2011). Besides its inherent biocompatibility, HA as a biomaterial presents interesting physicochemical properties for its application across a range of disciplines, from tissue engineering to cosmetic materials. (Burdick & Prestwich, 2011)

HA molecules are a chain of alternating units of disaccharide β-1,4-D-glucuronic acid - β-1,3-*N*-acetyl-D-glucosamine, forming a polysaccharide with varying molecular weight (MW). In the body, the MW of HA ranges from 100 kDa in serum to 8000 kDa in the vitreous. HA may be classified based on MW, namely low molecular weight HA (LMW-HA, 10–250 × 1 kDa), medium molecular weight HA (MMW-HA, 250–100 kDa), high molecular weight HA (HMW-HA, >1000 kDa), and very high-molecular weight HA (vHMW-HA, > 6000 kDa). (Tavianatou et al., 2019) HA has been found to have biological activity, playing a role in cell signaling pathways via specific cell-surface glycoproteins, inflammatory responses, and angiogenesis (Rayahin et al., 2015) . In materials science, it is often used as a building block known for its high-water retention ability and viscoelastic mechanical properties. (Kobayashi et al., 1994)

While it can form hydrogel networks within itself through hydrogen bonds, pristine HA is not suitable for bioink development, due to a high prevalence of the viscous modulus with limited shape retention upon printing. One can find HA to be the main component of the bioink, or as a viscosity enhancer. (Abbadessa et al., 2016) There are numerous chemical modifications that are applied to HA chains, to allow certain crosslinking mechanisms, functionalize the chain to promote cell adhesion, and overall to enhance its mechanical properties. (Highley et al., 2016) Methacrylate derivatives are of extended use to allow photo-crosslinking of many polymers, including HA (Kufelt et al., 2014). It is also common to combine HA with synthetic

polymers, although these strategies compromise biocompatibility and biodegradability. (Petta et al., 2018) HA as the main component of bioinks is rare, though it is possible to find it for hydrogels where enhanced mechanical properties (e.g., stiffness) are desired. HA-only bioinks have been applied with modifications via click chemistry for corneal 3D-printing (Mörö et al., 2023), combined HA derivatives (e.g., thermoresponsive and photosensitive) (Kesti et al., 2015), or modifications such as tyramine-conjugated HA (HA-Tyr) and acrylated HA. (Lee et al., 2018)

Combinations with other polymers are generally used and there are numerous examples. Skardal *et al.* mixed methacrylate HA (HAMA) with the methacrylated ethanolamine derivative of gelatin (ratio 4:1) and bioprinted it with human liver cancer cells. A partial photocrosslinking was applied before printing to enhance the ink viscosity, providing an extrudable formulation which was stabilized after printing by applying UV light again. (Skardal et al., 2010) HA-Tyr has also been combined with nanofibrillated cellulose to obtain a bioink that supported the printing of human-derived induced pluripotent stem cells, where the nanocellulose promotes a shear-thinning behavior and the HA acts as the bioactive component for adipose-like differentiation. (Henriksson et al., 2017)

Gelatin is another material that is extensively used in hydrogel systems. It is a biodegradable polypeptide resulted from partial hydrolysis of collagen (Figure 1.4), which is a fi-

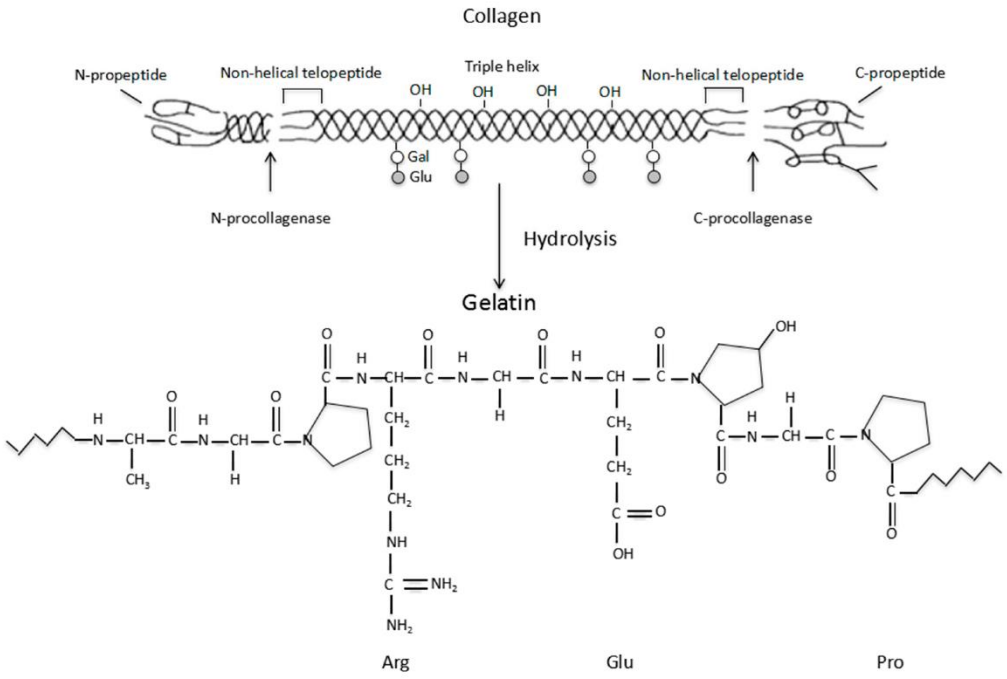

Figure 1.4. Schematic depiction of the collagen hydrolysis to gelatin. From Wang et al.. (2017)

brillar protein found throughout the body. Native collagen plays an important role in maintaining the integrity of the ECM in many tissues such as bones, cartilage, blood vessels and connective tissues. There exist several types of gelatins, depending on the hydrolytic treatment and source. (Wang et al., 2017)

Commercially available gelatin for regenerative medicine applications often comes from pig and bovine tissues. It is rich in RGD (arginine-glycine-aspartic acid) triplets, which are domains that interact with cell-adhesion proteins. Gelatin is a water-soluble polymer that solubilizes best in aqueous solutions above 40˚C, and naturally transitions to a physical gel under 30˚C (Asim et al., 2023). Gelation temperature limits its application as is when physiological conditions are required (ca. 37˚C). Therefore, it is common to perform chemical modifications on gelatin to provide additional crosslinking to stabilize the structure. Methacrylate derived gelatin (GelMA) is one of the most used polymers in rapid prototyping through bioprinting. It has been used as a standalone material for bioprinting liver lobule-like structures (Fan et al., 2023) or myoblast encapsulation in enzymatically crosslinked GelMA combined with photocuring. (Zhou et al., 2019) Unmodified gelatin may also be used as sacrifice bioink, to provide spatial separation among other bioinks, but easily dissolved and removed after printing (S. Liu et al., 2022). Several methods for chemically-induced gelation, such as the use of glutaraldehyde and carbodiimides, have been investigated to avoid dissolution. However, such methods are difficult to apply to *in situ* gelation *in vivo* or to constructs containing living cells, due to the toxicity of the cross-linking agents (Mazaki et al., 2014; Ulubayram et al., 2002). Similarly to the application of HA, gelatin is often found as bioinks in combination with other polymers, namely alginate (Immohr et al., 2023; Koch et al., 2020) , fibrinogen (Dai et al., 2016; Rutz et al., 2015; Taymour et al., 2022), or hyaluronic acid. (Ma et al., 2016; Skardal et al., 2010)

Tyramine-conjugates and enzymatic crosslinking has been used for bioprinting with collagen and HA conjugates (Kang et al., 2022), HA-based cascade enzymatic crosslinking (Sakai et al., 2021), or HA-Tyr for attachment of bioactive conjugates (Lee et al., 2018). In the present study, the synthesis and characterization of tyramine-conjugated gelatin and hyaluronic acid bioinks to form enzymatically crosslinked via HRP/ H_2O_2 reaction is presented. To our knowledge, such a combination of materials and crosslinking has not been explored yet in the context of bioprinting. Previous work has focused on the application of this system for injectable hydrogels (Sanmartín-Masiá *et al.*, 2017; Vaca-González *et al.*, 2020) and the combination of HA and Gelatin at an 80/20 volumetric ratio has shown good results for the encapsulation of hepatocytes (Rodríguez Fernández, 2021). The translation of these towards a scalable bioprinting strategy is the main focus of the research presented in the following sections.

2

MATERIALS AND METHODS

2.1 Materials

Hyaluronic acid sodium salt from *Streptococcus equi*; Gelatin from porcine skin (Type A, gel strength 300), 2-(N-Morpholino)ethanesulfonic acid (NHS), tyramine hydrochloride (Tyr, 98%), N-hydroxysuccinimide (NHS, 98%), hydrogen peroxide solution 30% (w/w), glucose solution 1M, bovine serum albumin (BSA), dialysis membranes 12.400 MWCO, Hoechst 33342 and propidium iodide, were purchased from Sigma-Aldrich (USA). Sodium chloride was supplied by PANREAC, ITW (Spain). 1 -Ethyl-3-(3-dimethylaminopropyl)carbodiimide (EDC) was purchased from Iris BIOTECH (Germany). Dialysis membrane 3500 MWCO from Spectrum (USA). 0.2 μm Polyethersulfone (PES) vacuum filter unit, non-treated P6, P12 and P24 were purchased from (Avantor VWR); F12 Nutrient mixture (Ham, 1X), L15 cell culture medium, Dulbecco's phosphate buffered saline (dPBS) from GIBCO, ThermoFischer (USA). Texas Red conjugate and Oregon Green conjugate from Invitrogen, ThermoFischer ScientificL-Glutamine and fetal bovine serum (FBS) from Biochrome AG (Germany). Cellink START sacrifice ink from Cellink (Sweden).

2.2 Synthesis of HA-Tyr

For initial tests, low molecular weight hyaluronic acid (LMW-HA) was used following previous experiments(Poveda-Reyes et al., 2016; Vaca-González et al., 2020). LMW-HA (ca. 320 kDa) was obtained through acidic degradation of commercial HA, which has a high molecular weight (HMW), estimated around 1200 kDa (Poveda-Reyes et al., 2016). First, 500 mg of hyaluronic acid sodium salt were dissolved in 50 mL Mili-Q water, under stirring at 4°C for 24 h. Once fully dissolved, HCl is gently added to the HA solution until a pH of 0.5 is achieved,

then left at 37°C for 24 h. It was necessary to homogenize well every time HCl was added, since the HA solution was viscous. After 24 h, the degradation was neutralized by adjusting the pH to 7 adding NaOH, and the product is dialyzed to retain only hyaluronic acid. The dialysis employs a 3500 MWCO membrane, against distilled water for 72 h, changing the water 3 times per day. Once dialyzed, the LMW-HA solution was frozen at -80°C and then lyophilized (4 days) to be stored.

Just as for Gel-Tyr, tyramine grafting of HA would allow the addition of phenolic moieties for enzymatic crosslinking. In Figure 2.2 the grafting reaction for HA is depicted. The molar ratios of carboxyl, EDC, Tyr, and NHS were the following (Table 2.1):

Table 2.1. Molar ratios used for tyramine grafting reaction for HA

Tyr : COOH	EDC : COOH	EDC : Tyr	NHS : EDC
2 : 1	1 : 1	1 : 1	1 : 10

The same grafting protocol was applied almost indistinctly for LMW-HA and HMW-HA. To perform this, a buffer solution is prepared dissolving 350.6 mg of NaCl (PANREAC) in 40 mL (150 mM NaCl), followed by 2.16 g of MES (Sigma-Aldrich). The pH of the buffer was adjusted to 5.75 using NaOH. Then, 200 mg of HA (LMW or HMW) were dissolved in the buffer solution. LMW-HA required only 2 h until complete dissolution under stirring at room temperature, while HMW-HA was left stirring during 24 h at 4°C. During this process, the flasks containing HA were covered given the photosensitivity of the polymer. In the HA dissolution, 172.94 mg of tyramine hydrochloride were added and left to dissolve for 15-20 min at room temperature. The pH was checked and adjusted to 5.75, when necessary, since the tyramine can release protons once dissolved. Then, 5.72 mg of NHS and 95.44 mg of EDC were added, to catalyze and activate the reaction, respectively. The reaction was let to occur during 24 h at 37°C under stirring. After this, dialysis was performed using a 12.400 MWCO membrane (Sigma). First, 24 h against 150 mM NaCl (21.9 g in 3 L of distilled water), and then another 24 h in distilled water only. The dialysis solution was changed three times per day. Once dialyzed, the solution was sterilized by filtration through 0.2 μm filters. In the case of LMW-HA, regular polyethersulfone (PES) filter 0.2 μm coupled to a syringe were sufficient; HMW-HA required a vacuum pump coupled to the filter unit (Avantor VWR), since the solution was highly viscous. The filtered solutions were frozen at -80°C and then lyophilized in sterile flasks, attached separately to the freeze-drying equipment (Alpha 1-2 LO plus lyophilizer, *Christ Germany*) for 4 days, and stored sealed to preserve sterility.

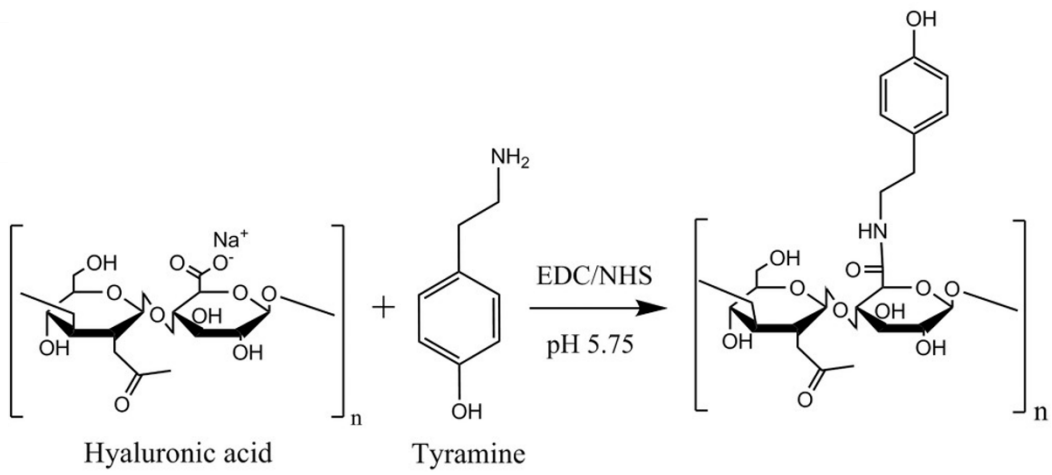

Figure 2.1. Grafting reaction of tyramine with hyaluronic acid chains via EDS/NHS forming amide bonds. Poveda-Reyes et al. (2016)

2.3 Synthesis of Gel-Tyr

The tyramine grafting of gelatin was performed using Sakai *et al.* protocol, further adapted by Sanmartín-Masiá *et al.* (Sakai et al., 2009; Sanmartín-Masiá et al., 2017) The molar ratios for each reactive group were selected as follows (Table 2.2):

Table 2.2. Molar ratios used for tyramine grafting reaction for gelatin.

Tyr : COOH	EDC : COOH	EDC : Tyr	NHS : EDC
2 : 1	2 : 1	1 : 1	1 : 10

This reaction consists of the replacement of carboxyl (-COOH) groups by tyramine groups, forming a bond with the amine groups of the tyramine by means of carbodiimide activation (EDC/NHS). In Figure 2.1 the grafting reaction is depicted. Ultimately, the phenolic groups of the tyramine allow the hydrogel crosslinking through an enzymatic reaction with HRP/H_2O_2.

For each batch of grafted gelatin (Gel-Tyr), a MES buffered solution 50mM was prepared by dissolving 195.24mg of MES (Sigma-Aldrich) in 20mL of Mili-Q water. Then, 0.4g of porcine gelatin A (Sigma-Aldrich) were dissolved in the buffer (20mg/mL Gelatin), under magnetic stirring at 60˚C for 30 min. Once fully dissolved, 111.13mg of tyramine hydrochloride (Sigma-Aldrich) were added, and the solution was left stirring at room temperature for 20 min. Next, the pH was adjusted to 6 by gently adding NaOH 0.1M drops alongside continuous stirring.

Following, 7.36 mg of NHS (Sigma-Aldrich) were added to dissolve during 30 min at room temperature, and finally 122.68mg of EDC (Iris BIOTECH) were added. The reaction solution was kept 24h at 37˚C. In order to remove unreacted reagents, dialysis is performed during 48h, using a 12.400 MWCO membrane (Sigma) in a 3L vase of distilled water, changed three times per day. Once dialyzed, the solution was frozen at -80˚C and then lyophilized to be stored.

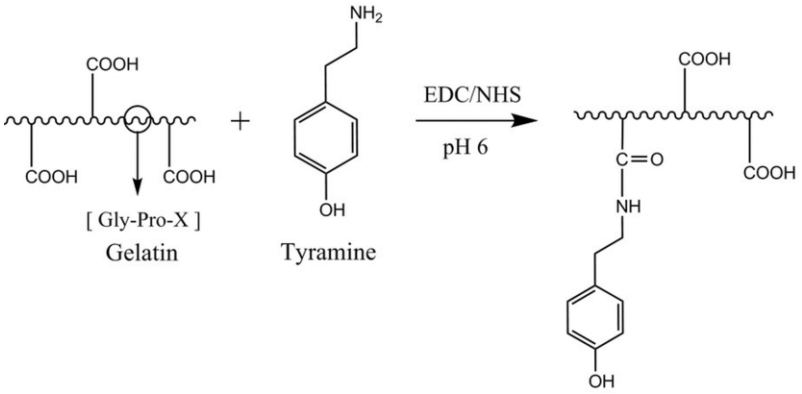

Figure 2.2. Grafting reaction of tyramine with Gelatin via EDS/NHS forming amide bonds. Poveda-Reyes et al. (2016)

2.4 Substitution degree of modified Gel-Tyr and HA-Tyr

The replacement of carboxyl groups by tyramine can be quantified as a percentage of phenolic moieties in the polymer chains. Both for hyaluronic acid and gelatin, when the grafting protocols are performed accordingly, the substitution degree is consistent among batches. The grafting characterization is performed as described by Poveda-Reyes et al. (2016). To characterize the substitution degree in HA, lyophilized HA-Tyr was prepared to 0.1% (w/w) by dissolving 1.5 mg in 1.5 mL of Mili-Q water., left to dissolve overnight at 4˚C.

Similarly, to characterize the substitution degree in Gel-Tyr, the lyophilized material was prepared to 0.1% (w/w) by dissolving 1.5 mg in 1.5 mL of Mili-Q water, ca. 30 min at 37˚C. The absorbance of the solution is measured at 275 nm (Cary 60 Uv-vis, Agilent), using a reference calibration curve of known tyramine concentration solutions. The phenyl group of the tyramine has strong absorption at 275 nm, whereas no signal for pure HA and Gel is expected at this wavelength.

The calibration curves for HA-Tyr and Gel-Tyr are the following *Equation 1* and *Equation 2*, with R^2 of 1 and 0.9989, respectively. *Equation 3* and *equation 4* simplify the calculation for the substitution degree. HA-Tyr and Gel-Tyr vary on the number of COOH per mg of material ($2.49 \cdot 10^{-3}$ and $0.8 \cdot 10^{-3}$ mM COOH/mg, respectively), which is calculated and from an

NMR-based model for HA and from the information provided by the supplier for the gelatin.The molecular weight of tyramine (MW_{Tyr}) is 137.18 g/mol. Ultimately, the substitution degree represents the number of tyramine molecules per 100 COOH molecules. (Darr & Calabro, 2009; Poveda-Reyes et al., 2016)

$$(1) \qquad \text{Abs}_{275} = 4.7917 \cdot [\text{Tyr}]_{Gel}$$

$$(2) \qquad \text{Abs}_{275} = 4.0939 \cdot [\text{Tyr}]_{HA}$$

$$(3) \qquad Substitution\ degree\ \%\ (Gel) = \frac{[\text{Tyr}]_{Gel}}{MW_{Tyr} \cdot 0.8 \cdot 10^{-3}} \cdot 100$$

$$(4) \qquad Substitution\ degree\ \%\ (HA) = \frac{[\text{Tyr}]_{HA}}{MW_{Tyr} \cdot 2.49 \cdot 10^{-3}} \cdot 100$$

2.5 Hydrogel formation tests

The reticulation ability of the hydrogels of every new batch of HA and Gel modified was assessed by incorporating the material and the crosslinking agents in a 100 µL drop. For every drop, 80 µL were the polymer (HA LMW-Tyr, HA HMW-Tyr or Gel-Tyr), 10 µL of HRP 12.5 U/mL, and 10 µL of H_2O_2 20 mM. Briefly, the polymer was dissolved at 4% (HA LMW-Tyr), 2% (HA HMW-Tyr) and 1% (Gel-Tyr) in F12 culture medium. Enough volume was prepared to at least produce 3 drops of hydrogel (ca. 320 µL of polymer solution). The polymer solution was then mixed with the HRP (40 µL of HRP for 320 µL of polymer). A drop of 90 µL was placed onto a parafilm-covered glass plate, and then 10 µL of H_2O_2 added from above. The drop of hydrogels were incubated at 37°C for 5-10 min and the gelation was visually confirmed.

2.6 Viscosity measurements

Rheological measurements of HA solutions (in F12), and the solutions formed by a mixture of HA and Gel were performed on a rotational shear rheometer. Rotational shear-viscosity measurements were performed in flow mode with shear rate ranging from 0.001 to 1000 s^{-1}. The sample to be measured was placed on the bottom plate, while the parallel top plate (diameter = 20 mm) was adjusted in height to reach sufficient contact with the drop of material.

The volume deposited was ca. 350 µL, and the gap between plates adjusted to the deposited volume ensuring maximum contact of the upper plate and the drop of material. The temperature of the plate was controlled and maintained, and measurements were always carried out at 37°C. Measurements were made in rotational rheometer Discovery HR-2 Hybrid (*TA Instruments*) and processed with TRIOS software (*TA Instruments).* The solutions characterized are shown below in table 2.3.

Table 2.3. F12 bioinks solutions evaluated in rheological characterization.

Polymer (s)	Concentration (% w/v)	Composition
HA HMW-Tyr	1	100
	2	
	3	
	4	
	5	
HA HMW-Tyr / Gel-Tyr	4	80/20
	5	

The lyophilized polymers were dissolved in F12 cell culture medium. For the HA and HA/Gel mixtures, they were dissolved separately and mixed accordingly (80/20) using a syringe-to-syringe method to homogenize. CELLINK START is a water-soluble gel provided by the bioprinter manufacturer (Cellink, Sweden) and was also measured and considered as a control for optimal viscosity due to its excellent extrudability. The viscosity (Pa ·s) was represented against the shear rate applied (1/s), plotted using *Prism 8.0.2*. (GraphPad Software Inc.)

2.7 G-code modification

All 3D models were initially designed using FreeCAD 0.20.2 software. The models were exported as *stl* files to then be processed by *DNAStudio* slicer software (Cellink, Sweden). For the grid models, horizontal and vertical patterns were exported separately in order to be recognized by the slicer as single line trajectory patterns. This issue is illustrated in Figure 2.3. Other models designed for cell culture and miscibility assays were single and concentric circles. Concentric circles were designed, processed, and printed separately, unlike the grid model where vertical and horizontal patterns were combined into a single G-code file post-processing.

To achieve in demand crosslinking, the combined use of a bioink (polymer, HRP, and cells) and the crosslinking agent (H_2O_2) in separate printheads was programmed in the G-code. The slicer processing only accounts for one printhead. Thus, the output G-code was modified (Figure 2.4) to double and insert a layer of the second printhead (EMD in this case), following the same path as the previous layer.

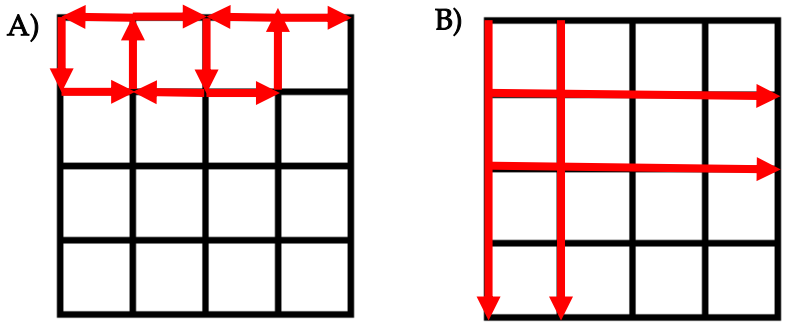

Figure 2.3. Illustrated issue in printing trajectory. When processing whole grid model through slicer (A), each arrow translating into a line of code and more complicated path. When vertical and horizontal models are processed separately and then the code combined, the output trajectory is simplified (B).

As shown in Figure 2.4, the line of command previous to the coordinates is modified from T0 (first printhead) to T2 (second printhead). G1 are extrusion commands, in which first the Z parameter determines the height of extrusion for each layer, X and Y the relative distances to move while extruding in the x/y plane. On the other hand, F and E commands indicate the feed rate and mm of material extruded respectively, and these are not modified after processing. Ultimately, the speed and extrusion pressure were directly controlled in the printer's console. Another parameter modified when implementing both printheads was to set the second printhead T1 (EMD) to a fixed relative height of Z0 for all layers. Thus, the EMD printhead remained always at the height defined when calibrated, above the wells of the plate.

Another consideration taken into account for the CAD design of the models was that the model strands had to be 0.01 mm below the desired gauge to avoid an issue with the processing software. Thus, models for 20G (inner diameter 0.60 mm) and 22G (inner diameter 0.41 mm) were designed with a strand thickness of 0.59 mm and 0.40 mm, respectively.

The number of layers of the final structure was defined by the processing software, considering the *stl* model height (e.g., 3 mm) and the desired gauge. For a 3 mm tall structure, using a 20G gauge (0.60 mm), five layers of polymer were printed (3 mm/0.60 mm = 5 layers), while for 22G gauge (0.41 mm), seven layers of polymer were printed (3 mm/0.41 mm ≈ 7 layers).

Figure 2.4. Modification example of G-code. Left, G-code as exported from slicer software. Right, manually inserted sections (green) to define printhead change from T0 to T1 and fix the Z position (red). The trajectory followed by T1 printhead is the same as the previous layer by T0. All text after ";" are comments for ease of understanding by the user.

2.8 Printability evaluation

Printability refers to the capacity to form and maintain a reproducible three-dimensional structure, according to a CAD-designed model. Printability was evaluated here based on extrudability, strand uniformity, and pore factor. Briefly, extrudability was assessed by testing whether it was possible to eject material through the nozzle (22G) at a certain pressure up to the maximum pressure achievable (200 kPa) by the *Cellink BIOX* printer. Both uniformity and pore factor were evaluated with a 4 x 4 (30 x 30 x 3 mm) square grid design, with a 0.4 mm strand thickness to fit a 22G nozzle. The inner squares are designed to be 7 x 7 mm (49 mm^2). Pictures of the grid were taken using a simple magnification microscope (RS Pro Portable Stand Alone Microscope) and images analyzed with *ImageJ*. Grids printed with CELLINK START (Cellink, Sweden) were used as a control for its excellent extrudability and apparent resolution of the structures printed.

Uniformity was measured as a ratio of average strand width measurements (n = 25) and the average of the strand thickness of the control grids. Thus, values above 1 represent thicker strands than the control, and closer values to 1 would be considered more uniform.

The pore factor was measured as a ratio of the average pore area i.e., grid inner squares (n = 4) and the average pore area of the control grids. In this case, values below 1 imply reduced pore area compared to the control.

Printability was evaluated for all HA HMW-Tyr and its mixtures with Gel, HA/Gel, (Table 2.3). The grids were printed on glass plates, with a controlled printhead and print bed temperature of 37°C. The CELLINK START controls were printed from the cartridge as is.

During the extrudability evaluation, the minimum pressure required for each mixture was also evaluated. For HA-based inks, the HA was directly dissolved in the 3 mL cartridges in F12 media. Gel was dissolved in Eppendorf separately. For the mixtures, Gel and HRP (12.5 U/mL) were introduced altogether to the cartridge and homogenized with the HA. The cartridges contained 90% of polymer solution (HA or HA/Gel) and 10% of HRP 12.5 U/mL. The EMD printhead (valve) was setup at 37°C and loaded with a H_2O_2 20 mM cartridge (diluted in F12 culture media), and after every layer of ink, this printhead deposited the peroxide on the printed pattern. The EMD valve deposited drops by opening the valve 1 ms every 80 ms.

2.9 Bioinks miscibility/non-miscibility assay

To test whether bioink candidates could be printed in close contact while maintaining separate stable structures, concentric circles with a varying distance gap were printed. Considering that our bioinks form hydrogel networks, swelling of the printed structures when immersed in culture media is also expected, potentially increasing the contact area between two structures. Bioprinted structures in contact can be explored for co-culture models. For this assay, two blends of the HA-Gel mixtures were used: HA HMW-Gel 4% 80/20 and HA HMW-Gel 5% 80/20. The bioinks were mixed with two distinct fluorophores, Texas Red and Oregon Green (Invitrogen, Thermo Fisher Scientific) and dispersed in the solution at a concentration of 200 µg/mL. The fluorophores provided by the supplier were dissolved in PBS/azide 0.05% to a concentration of 1 mg/mL and kept frozen in aliquots of 200 µL.
The cartridges were prepared as follows: 500 µL HA HMW-Tyr, 125 µL Gel-Tyr, 62.5 µL HRP 12.5 U/mL and 137.4 µL fluorophore 1mg/mL (V_t = 824.9 µL). The HA HMW-Tyr was previously let to dissolve in the cartridge for 3 days at 4°C, with its final volume (500 µL) of F12 media at the concentration desired (4% or 5%). Gel-Tyr was dissolved in F12 at each concentration separately in Eppendorfs during 30 min at 37°C. The EMD cartridge was freshly prepared with H_2O_2 20 mM in F12 media. The dissolved HA was homogenized with Gel, HRP 12.5U/mL solution and fluorophore. The printing process was performed in the dark, and at a controlled temperature of 37°C in printheads and print bed. A 20G (0.60 mm) nozzle was used and the CAD models were designed consistently, so that the strand thickness modelled was 0.59 mm, and each gap would be a multiple strand thickness (Figure 2.5).

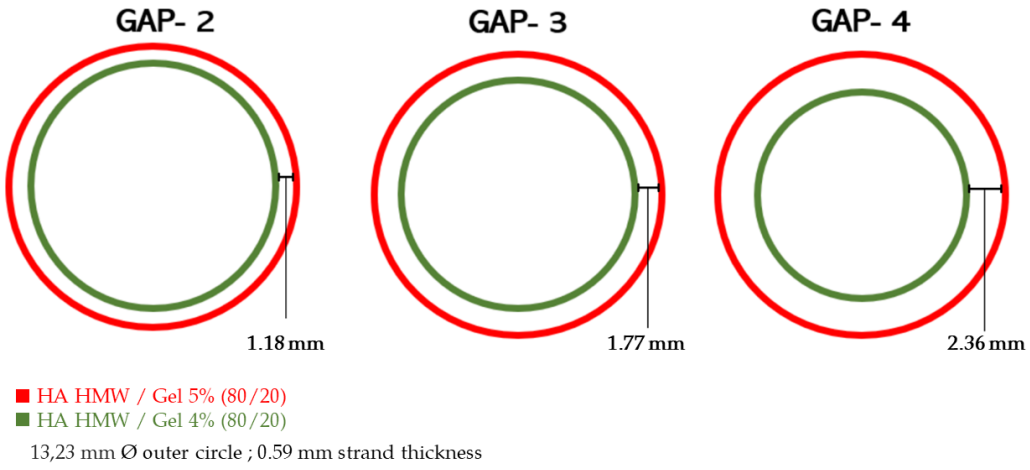

Figure 2.5. CAD models used for miscibility assay. All outer circles have a 13.23 mm diameter, while the inner circles vary in the gap with the outer one. The gap is proportional to the strand thickness considered (0.59 mm) to use a 20G nozzle.

The constructs had a modeled height of 3 mm (5 layers of bioink). The outer and inner circles were two independent models fully printed independently. Three replicas of concentric circles for each gap were printed on a P12 plate and imaged under Leica DMI8 inverted microscope (Leica microsystems, Germany) after printing, and after incubation during 24 h in F12 culture media at 37˚C.

2.10 Bioprinting and cell culture

2.10.1 Bioprinting of cylindrical constructs

Hepatocarcinoma cells (HepG2) were encapsulated in 3D printed constructs using two of the bioinks developed: HA HMW-Gel 4% 80/20 and HA HMW-Gel 5% 80/20. Two sizes of nozzle diameter, 22G and 20G, were used to evaluate its possible impact on cell viability. The HepG2 cells used were provided by the Experimental Hepatology Unit, Health Research Institute La Fe, Valencia, Spain. Non-sterile material was treated with autoclave, including cartridges, plunges and luer locks. Lyophilized HA HMW-Tyr was let to dissolve for 3 days at 4˚C in F12 cell culture media in separate cartridges for each concentration of 4% and 5%. Lyophilized non-sterile gelatin was first dissolved in a falcon tube at the specified concentration, during 1 h at 37˚C. Once dissolved, it was filtered through 0.22 µm polyethylsulfone (PES) syringe filters.

Table 2.4. Range of pressures applied during bioprinting of cell-laden bioinks.

	Concentration	
Nozzle gauge	HA HMW/Gel 4%	HA HMW/Gel 5%
22G	100 - 110 kPa	110 - 120 kPa
20G	70 – 80 kPa	90 - 100 kPa

HepG2 cells were provided by the source laboratory and had been expanded in T75 flasks. For the seeding, first the medium was removed from the flasks and subsequently washed with DPBS. Briefly, HepG2 culture media was prepared as follows for a ± 100 mL volume of media: a mixture of 50 mL F12 and 50 mL of L15 culture media was supplemented with 7 mL FBS, 2 mL of BSA (100 mg/mL), 1 mL of Penicillin -Streptomycin, 1 mL of L-glutamine, 0.5 mL of glucose 1 M, and 1.2 mL of sodium bicarbonate. To detach cells from the flask, 1 mL of trypsin was added and let to incubate for 3-4 min at 37°C. Next, the trypsin was inactivated by adding 10 mL of HepG2 cell culture media, and the whole volume centrifuged in a falcon tube at 1500 rpm during 3 min. Then, the supernatant was removed, and the pellet was resuspended in 10 mL of culture media. 10 µL of the cell suspension were loaded onto a Neubauer chamber to count and estimate cell density. Our desired cell density within the bioink is of 2×10^6 cells/mL. Therefore, considering we were filling completely our 3 mL cartridges, $6 \cdot \times 10^6$ cells were required per cartridge (n= 4). The volume of cell suspension required to have that amount of cells was centrifuged, the supernatant discarded, and the pellet resuspended in the filtered Gel-Tyr solution and HRP 12.5 U/mL. Thus, the mixture of cells, gelatin and HRP was ready to be homogenized together with the HA HMW in the cartridge.

The bioprinter inner chamber was sterilized using its own UV program, and the laminar flow fan was on during the whole printing process. The printheads and print bed were pre-heated at 37°C.

For each composition, the cartridge containing HA/Gel/HRP/HepG2 was loaded in the first position printhead, and a sterile solution of H_2O_2 in F12 culture media was loaded in the second printhead (EMD type). Cylindrical models of 15 mm diameter and 3 mm in height were printed in several P6 plates, at least 3 replicas per condition. The diameter of the cylinders

was designed to fit in P12 plates, with enough space between the well walls and the structure to ensure good immersion in cell culture media after printing. The printing pressure was the main parameter varying among conditions, as shown in Table 2.4. For all constructs, a pre-flow of 300 ms was set (e.g., time in which the extrusion starts ahead of the model). After printing, the plates were incubated at 37°C for 15 to 30 min to let the hydrogels to properly crosslink. Next, 4 mL of HepG2 culture media were added to each well and maintained at 37°C.

2.10.2 Assessment of cell viability

The cell viability in the constructs was evaluated at day 0 and day 1 through live/dead staining. First, the culture media was removed from the wells of the plate. Fluorescent probes Hoechst 33342 and Propidium iodide were used to indicate the presence of live and dead cells, respectively. While Hoechst 33342 is a cell-permeable blue probe that binds to adenine-thymine regions of DNA, propidium iodide is a red probe that only permeates in dead cells and intercalates between the DNA bases. A mixture of both fluorophores was prepared in HepG2 culture media with a concentration of 1.5 µL marker/mL. The constructs were incubated with 4 mL of probe mixture for 30 min at 37°C protected from light.

After incubation, the probe mixture was removed and replaced with HepG2 culture media, and imaged with fluorescence microscope Eclipse 80i (Nikon, Japan) under red and green filters. The images were obtained for each channel separately and were processed and combined with FIJI software (ImageJ), performing background correction accordingly and automatic cell count.

2.11 Statistical analysis

Statistical analysis was performed using GraphPad Prism 8. Two-way ANOVA test was applied to cell viability results. *P-values < 0.05, **P-values < 0.01, and *** P-values < 0.001 were statistically significant. Error propagation rules (Farrance & Frenkel, 2012) were followed to compute the standard deviation of uniformity and pore factor. A ratio (Q) of average measurements (a and b), has an associated error δQ computed from δa and δb (standard deviation of a and b, respectively). Error propagation for division considers the following rule (5):

$$(5) \quad Q = \frac{a}{b} \quad ; \quad \frac{\delta Q}{|Q|} = \sqrt[2]{(\frac{\delta a}{a})^2 + (\frac{\delta b}{b})^2}$$

3

Results and Discussion

3.1 Gel formation and grafting degree

The tyramine grafting is essential for the gelation of our HA-based bioinks, as well as for the crosslinking of both HA and Gel polymer chains. While Gel has a temperature-sensitive gelation under 23˚C, this is a reversible physical crosslinking, which can become unstable when the temperature is increased to 37˚C, resulting in solubilization of the hydrogel. Hence, chemical modification of gelatin is a common practice to enhance gelatin hydrogel stability. On the other hand, while pristine HA may be applied in combination with other components for tissue engineering platforms, HA-based hydrogels often incorporate some chemical modification that allows it to form mechanically stable networks while enhancing its swelling ability (Ouyang et al., 2016; Sanmartín-Masiá et al., 2017)

Gel and HA were chemically modified by grafting their carboxylic groups with the tyramine amine group by means of an EDC-NHS catalyzed reaction. For each batch synthesized, we assessed its ability to form a gel using HRP and H_2O_2 and evaluated the substitution degree with tyramine groups. While in previous work the grafting and hydrogels were produced using HA LMW, resulting from acidic degradation (Poveda-Reyes et al., 2016; Vaca-González et al., 2020), in this work we applied the same reaction to non-degraded HA (HA HMW), and evaluated whether the grafting and gelation ability were consistent.

A previous study reported a tyramine grafting degree of 7% for HA, and 24% for modified Gel (Poveda-Reyes et al., 2016). Furthermore, it was reported that the tyramine reaction reduced the molecular weight of both gelatin and HA (Sanmartín-Masiá et al., 2017). In this study, all batches analyzed showed a consistent grafting degree of ca. 6% for HA LMW, and 7% for HA HMW, and 20% for Gel. Simultaneously, a small hydrogel drop of 2% HA or 1% Gel was produced (adding HRP and H_2O_2) to visually confirm the gelation ability.

3.2 Rheological characterization

Inks for bioprinting need to fulfil several key requirements for processing with a 3D bioprinter. The main challenge is that they need to be printable, and then meet criteria desired for their application in tissue engineering and regenerative medicine. We screened several bioinks with potential applications for bioprinting with varying HA molecular weight (LMW or HMW), HA concentration, and incorporating Gel at a 80/20 (HA/Gel) ratio. Our first assessment was to perform rheological measurements on these bioinks, specifically shear viscosity tests, to evaluate the shear-thinning properties of the material, and its shear behavior, which is key for extrusion-based bioprinting. We started preparing solutions of HA LMW at 10, 15 and 20% (w/v) since it had been used to form hydrogels (2% w/v) and encapsulate primary hepatic cells in previous work (Rodríguez Fernández, 2021). HA LMW formulations were, however, dismissed for further study since they required a substantial amount of lyophilized material, and its overall viscosity was significantly lower than the lowest concentrations of HA HMW.

In addition, Cellink START ink was used as our control to approach due to its excellent printability. We differentiated two regions in the viscosity measurements (Figure 3.1): zero-shear zone and shear stress zone. The region that informs us the most about the ink behavior upon extrusion conditions is the shear stress zone. Therefore, differences in the zero-shear zone are a mere indicator of the ink viscosity as is, which is nevertheless an important factor to consider especially for manipulation purpose, such as pipetting difficulty or achieving a homogenous mixture with other components. All inks studied present a shear-thinning behavior, as seen by the descending curves in Figure 3.1, where the viscosity is reduced when applying a shear stress. Non-shear thinning (i.e., shear thickening) behavior would difficult or even fully prevent the extrusion of the ink through the nozzle. It is worth noting that HA HMW 5% was deemed maximum concentration to be studied given that its apparent high viscosity was already hard to work with. Interestingly, it was observed that none of our formulations reached a zero-shear viscosity as high as the control. However, if we look at the shear stress zone, in Figure 3.1A we can see that the viscosity values increase and approach the control as the concentration of HA increases, to a point where HA HMW 4% and HA HMW 5% overlap and even surpass the control between 10 and 1000 s^{-1}. HA HMW 3% has the closest shear stress behavior to the control. Given these results, we proceeded to test the blends of HA HMW 4 and 5% with Gel, which we would expect would reduce the viscosity of pure HA inks and could help tune the behavior during extrusion.

As seen in Figure 3.1B, with the addition of gelatin to HA HMW inks, the HA-Gel 4% resembles the HA HMW 3% behavior both in zero-shear and shear stress zones. Given that HA HMW 3% has the closest behavior to the Cellink control, we can infer that HA-Gel 4% will too have an optimal performance in the printing process. As for HA-Gel 5%, we observe a reduced zero-shear viscosity compared to pure HA HMW 5%, more similar to HA HMW 4% instead. However, the shear stress curve does still overlap with the highest concentrations of HA. Based on these results, we could proceed to test whether this measured behavior would correspond to its extrudability ability.

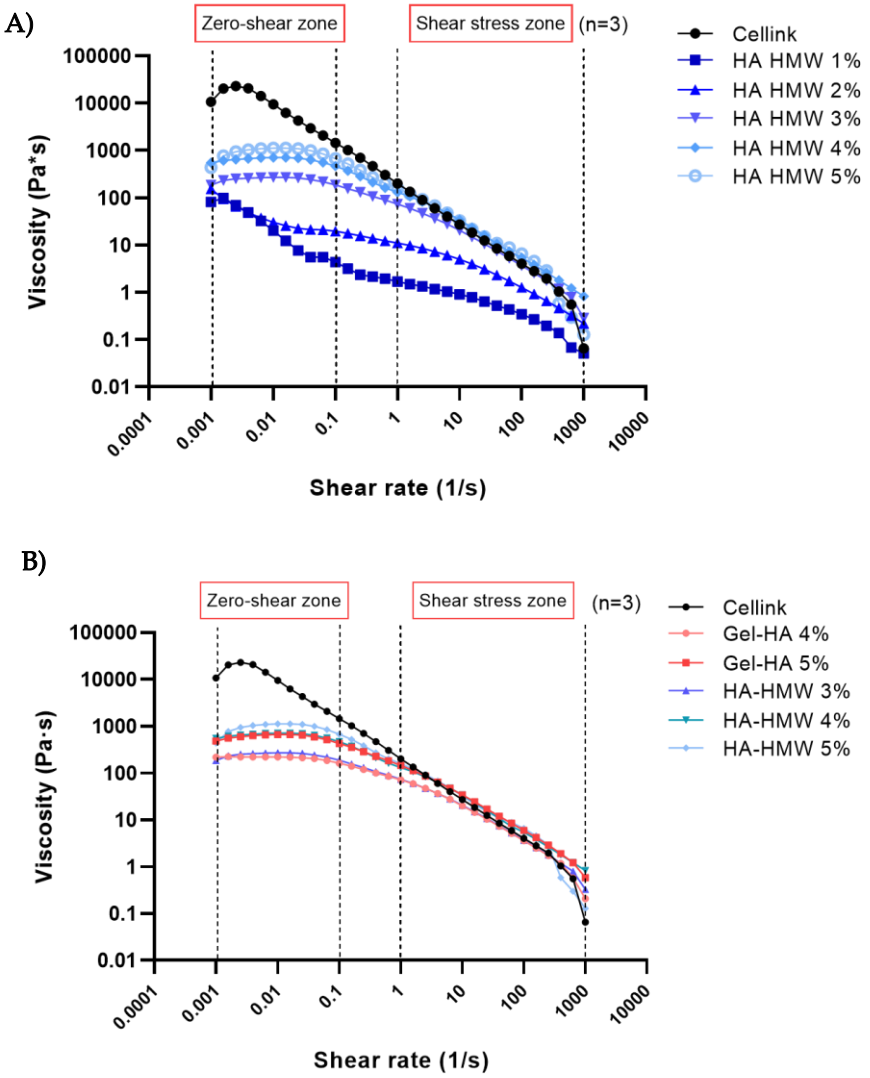

Figure 3.1. Shear viscosity measurements. (A) HMW HA 1-5% and Cellink START bioink, and (B) HMW HA and Gel at a 80/20 volumetric ratio. The bioink behavior expected upon extrusion corresponds with the decreasing viscosity in the shear stress zone.

Furthermore, this viscosity behavior represents the polymeric fraction of the bioink only, while the complete formulation would include a small volume of HRP for crosslinking, and

cells. The incorporation of cells has been shown to decrease viscosity of the polymer-based ink. Nevertheless, some studies suggest that increasingly high concentration of cells (> 10^7 cells/mL) in suspension can increase bioink viscosity (Blaeser et al., 2016). This relationship will, however, depend on the polymers used, type of cells, and range of viscosities. In this study, we did not evaluate the rheological properties of the cell-laden bioinks, but it is worth noting that cells were added in a suspension with the dissolved gelatin and HRP fraction, to avoid adding extra volumes.

3.3 Printability

Printability comprises a set of parameters that ultimately define the quality of the printed construct. Generally, bioinks with higher viscosity maintain its shape better; however, higher shear forces applied consequently might seriously affect the viability of the cells involved. (Naghieh & Chen, 2021; Webb & Doyle, 2017) The first parameter to consider is the ability of the bioink to be ejected through the nozzle, namely extrudability. Viscosity is the main feature that can be associated to extrudability, and higher viscosities will require increased pressure or force to extrude the solution. (Paxton et al., 2017) While normally, pneumatic extrusion-based bioprinting is suitable for viscosities ranging from 30 10^{-3} to 6 10^4 Pa·s (Kyle et al., 2017) , this will depend on the range of pressures that the printer can reach.

We evaluated the extrudability of all bioinks within the whole range of pressures achievable by Cellink BioX bioprinter (1-200 kPa) up to the minimum pressure required to observe a filament-like extrusion through the nozzle (22G). The minimum pressure (kPa) required for each concentration and composition tested is shown in Table 3.1. We can indeed notice that an increase in the HA concentration requires higher pressures, which correlates with its increasing viscosity. Likewise, the incorporation of Gel to the bioink, at a 80/20 (HA/Gel) volumetric mixture, reduces the printing pressure required according to its reduced viscosity. HA 5% was not extrudable at pressures ≤ 200 kPa using a 22G nozzle and was thus not considered for further evaluation of its printability. However, the mixture of HA-Gel 5% was successfully extruded, hence HA 5% could be considered as a precursor to dilute and tune the composition.

Next, we evaluated the uniformity and pore factor, as other printability parameters of the bioink. Grid constructs (4 x 4 ; 30 x 30 x 3 mm) were printed for each bioink. Crosslinking was initiated with the presence of HRP within the bioink, and H_2O_2 20 mM dispensed by drops over the pattern in each layer. Uniformity is a parameter defined by the closeness of the

printed strand width to the optimal strand width. Aqueous inks are going to have some dispersion of the strand compared to the model. While usually this optimal considered might be the strand width in the model (e.g., 0.41 mm), in this case we compared with the Cellink START ink as our control for its excellent printability. The width modeled was 0.41 mm (22G), while the average width of the control was 0.72 ± 0.05 mm. The area of the modelled squares was 49 mm^2, and the control was 41.90 ± 0.61 mm^2.

Table 3.1. Minimum extrusion pressures for tested bioinks. HA 1-4% and 80/20 HA-Gel 4-5%

Bioink	Min. extrusion pressure (kPa)
HA 1%	10
HA 2%	50
HA 3%	100
HA 4%	125
HA 5%	(not extrudable)
HA-Gel 4%	95
HA-Gel 5%	160

The average width of the printed strands were divided by the average of the control width ($\bar{W}_i / \bar{W}_{Control}$; n = 25). From zoomed out images of the same constructs, the pore factor was computed as the ratio of areas ($\bar{A}_i / \bar{A}_{Control}$; n = 4). In both cases, values closer to 1 are considered to have improved uniformity and pore factor, respectively. The way these measurements were done is shown in Figure 3.2A. Both parameters are complementary and can be understood as the resolution of the final construct. Some articles define the pore factor with a ratio of perimeter/area (Naghieh & Chen, 2021; Sarker et al., 2018). However, we found that this ratio can be misleading, since this ratio can give the optimal 1 when a perimeter of a printed construct is highly irregular and the area is reduced, yet the relationship between both remains close to the optimal. Other authors have used the ratio of perimeters with their theoretical optimal (e.g., 3D model) to measure the pore resolution. (Ouyang et al., 2016) Other studies have also proposed that the standard deviation of the measurements is in itself an indication of uniformity. (Göhl et al., 2018) Our approach is therefore a combination of the two latter ones, while considering areas instead of perimeters for the pore resolution.

It is readily noticeable that an increase in the HA concentration yields more uniform constructs (Figure 3.2 B-C). The reason why HA 1% seems more uniform than HA 2% might be due to a finer tuning of the pressure/viscosity balance, but both are highly irregular as it can be inferred from the high standard deviation on these measurements when compared with

the increasing HA content in HA 3% and HA 4%. It is worth noting that HA 4%, despite displaying a higher viscosity upon shear stress (Figure 3.1) than the control, almost overlapping with HA 5%, it was extrudable (unlike HA 5%) and presented the highest uniformity and pore factor of all HA-based inks.

The incorporation of Gel to the HA solutions yields constructs with higher strand uniformity. The bubbles observed within the constructs are caused by the mixing (syringe-to-syringe) with the gelatin (Figure 3.2 B-C). Letting the loaded cartridges after mixing in an ultrasound bath for 30 min had no noticeable effect in the bubble content and bubble cavitation might have an impact on cell viability when cells are also incorporated in the mixture.

From the comparison of uniformity and pore factor ratios, we can see that they are mostly consistent, approaching 1 in both cases. Nevertheless, we observe that for HA-Gel mixtures, while strand uniformity gets closer to the control, the pore factor is reduced subsequently. Despite the observable improved uniformity with the increase of polymer concentration, we observe that HA-Gel 5% does have a much higher standard deviation in its measurements, which could then be related to the reduction in pore factor. This difference could be attributed to an irregular deposition of more viscous bioinks, where material tends to accumulate in the grid nodes, hence reducing the overall area.

A starting point to choose a bioink can be these printability parameters, and based on our results, HA-only inks between 3 and 4%, and HA-Gel 80/20 mixtures at 4% and 5% are extrudable and show good strand uniformity and pore factor, in both cases improved by the increased polymer concentration. In contrast, the incorporation of Gel reduces the pressure required to extrude at the cost of reducing the pore factor potentially due to bubbles and ink dispersion at the nodes. While HA accounts for the main component of these bioinks and is responsible for the high viscosity and stiffness of the printed hydrogels, Gel can be used as a component to tune down the viscosity of the bioinks and ultimately the stiffness of HA-based hydrogels, while also favoring cell adhesion. (Poveda-Reyes et al., 2016; Sanmartín-Masiá et al., 2017)

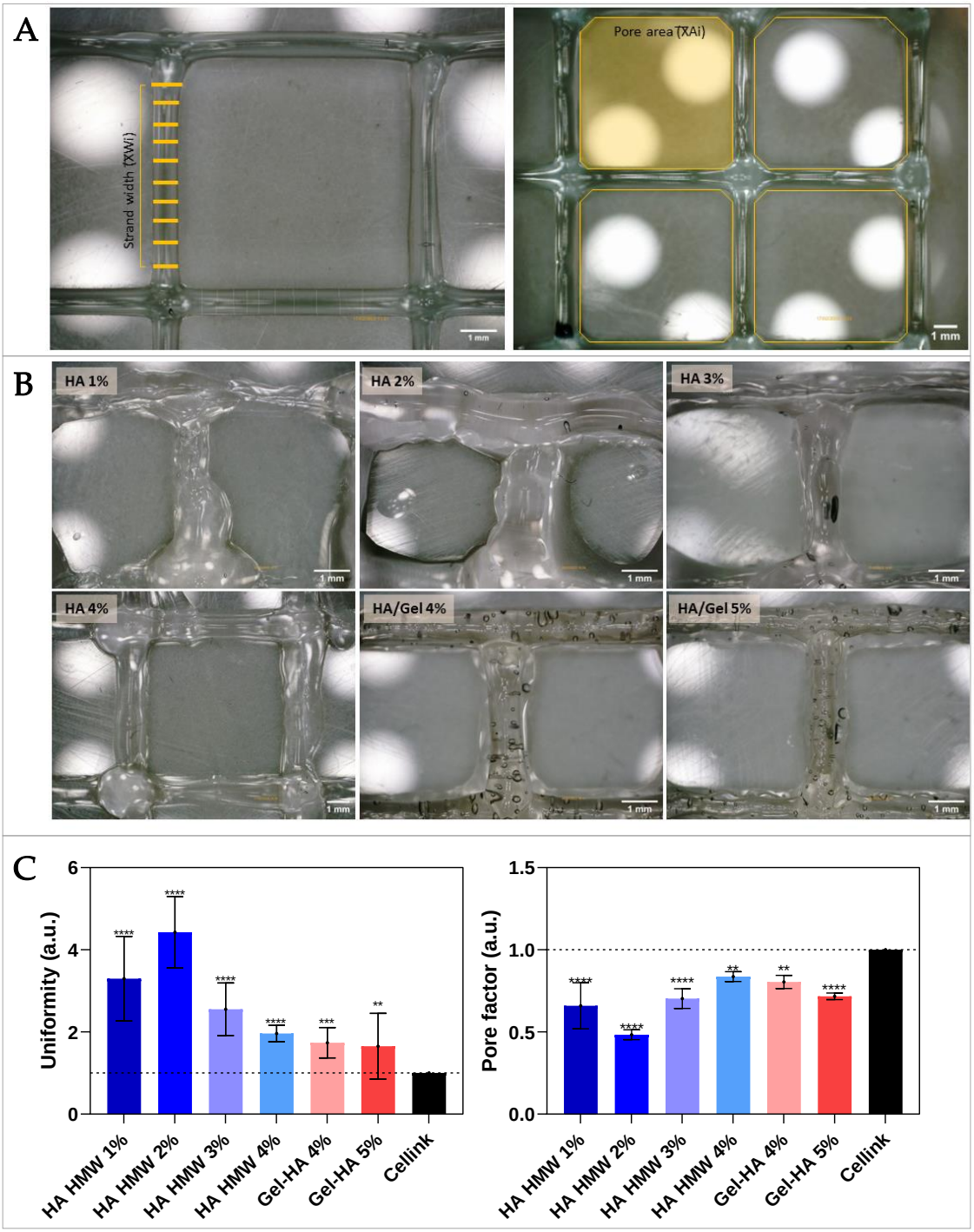

Figure 3.2. Printability evaluation. Measurements on Cellink START control constructs (A) for strand width (left) and pore area (right). A total of 25 width measurements and 4 pore areas were considered for every grid. Printed constructs for our tested bioinks HA 1-4%, and 80/20 HA-Gel 4% and 5% (B). Uniformity and pore factor ratios (C), where Cellink START is considered the control ($U_{Cellink}$ = 1; $PF_{Cellink}$= 1). Standard error of the ratios computed according to error propagation rules. One-way ANOVA analysis. P-values **** < 0.0001, *** < 0.001, ** < 0.01. Scale bar: 1mm.

3.4 Bioprinting of HepG2 cells

In this study, we wanted to focus on suitable 3D-printed supports for hepatic models. HA and Gel-based hydrogels have been previously used for hepatocarcinoma cell encapsulation (Hwang et al., 2010) , and bioprinted hepatocarcinoma models. (Ma et al., 2016)

After the characterization of our bioinks, we proceeded to incorporate cells to understand their suitability for cell encapsulation, as well as the tolerance to the bioprinting process as a whole (e.g., extrusion pressure, in demand crosslinking, etc.). Human hepatocarcinoma (HepG2) cells (Experimental Hepatology Unit, Health Research Institute La Fe, Valencia, Spain) were expanded in flasks and mixed in the bioink cartridges to a concentration of 2×10^6 cells/mL. Other studies encapsulated HepG2 cells within different polymer bioinks at concentrations ranging from 1.5×10^6 to 5×10^6 cells/mL (Billiet et al., 2014; Sun et al., 2020; Taymour et al., 2022), which is in the range of our selected concentration. It is worth noting that the addition of cells can change the viscosity of the bioink, hence influencing the parameters for the printing process.

For example, Blaeser *et al.* showed that cell concentrations over 1×10^6 cells/mL have a significant impact on alginate based bioinks, where higher cell numbers increase viscosity and amplify the shear thinning effect (Blaeser et al., 2016). In this study, we did not evaluate the effect of cells on the bioink properties. However, we did reduce the initial pressure range applied (Table 2.4) compared to the extrudability results with the polymers alone. Nevertheless, no additional volume was added with the cells since they were re-suspended to the desired concentration in a gelatin and HRP solution. Therefore, we hypothesize that the printing pressure difference might be due to a more sustained maintenance of the bioinks at 37˚C, since this was critical to ensure cell viability, while during the extrudability experiments, the cartridges were not kept under controlled temperature outside of the printheads. For bioprinting we applied a range of pressures rather than one single value, since small adjustments during the printing process (±10 kPa) to compensate for non-homogenous fractions in the bioink mixture.

Despite performing well in terms of printability, HA only bioinks were not considered for cell culture since optimally gelatin would provide adhesion sites through RGD domains. (Poveda-Reyes et al., 2016)

The two HA-Gel mixtures were printed into cylindrical constructs onto non-treated plates, with a diameter of 15 mm. Two different nozzle diameters (22G and 20G) were tested to evaluate the effect on the cells' tolerance to the printing process. In total, two conditions were tested: polymer concentration and nozzle gauge. As expected, by using a 20G nozzle the minimum pressure required for extrusion was reduced compared to the smaller diameter of 22G. For HA-Gel 4% it went from 100 kPa (22G) to 70 kPa (20G), while HA-Gel 5% from 110

kPa (22G) to 90 kPa (20G). After every layer, H_2O_2 20 mM was dispensed on the ring to cross-link the polymers in the bioink.

The viability of cells within the constructs was evaluated at day 0 (post-printing) and day 1. HepG2 cell culture media was introduced in the wells after printing to provide the necessary nutrients for the cells, while also allowing the rings to swell after the crosslinking. The live-dead assessment was carried out shortly after (ca. 30 min) and cells observed under a fluorescence microscope (Eclipse 80i, Nikon Japan). The viability was inferred from pictures of multiple rings (n = 3). In Figure 3.3, representative pictures of post-printing constructs are shown.

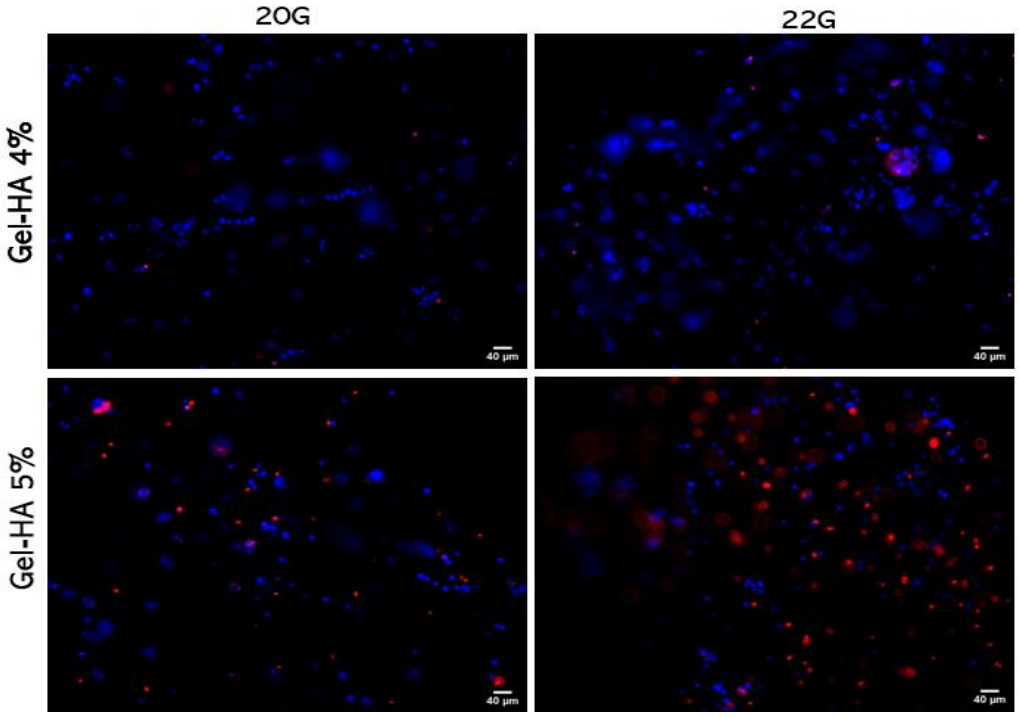

Figure 3.3. Post-printing day 0 viability. All nuclei (blue) stained with Hoechst 33342. Dead cells (red) stained with propidium iodide. Scale bar: 40 µM.

It can be observed that for both bioinks, there are more dead cells for 22G than for 20G. This can be explained by the reduced pressure applied as well as the nozzle diameter causing more shear stress on the cells when reduced from 20G to 22G. Likewise, a higher polymer concentration translates into higher extrusion pressures and more stress applied to the cells, both from the pressure but also from the polymer chains. Previous studies have reported loss of cell viability in HepG2 attributed to the increasing dispensing pressure and thinner nozzle diameter. (Chang et al., 2008).

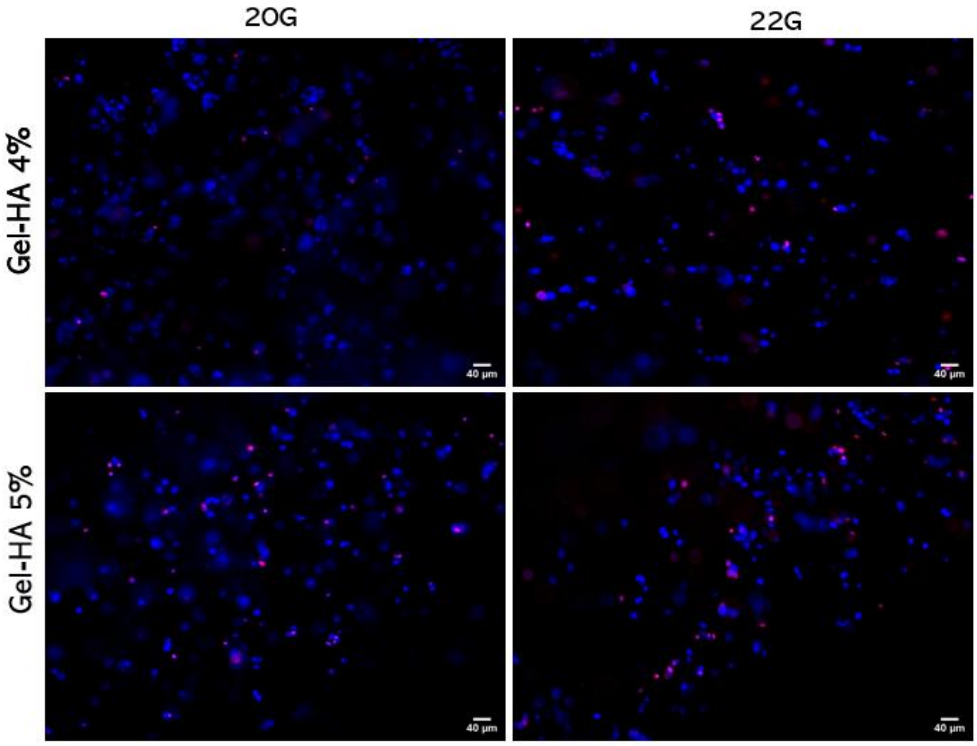

Figure 3.4. 24 h post-printing (day 1) viability. All nuclei (blue) stained with Hoechst 33342. Dead cells (red) stained with propidium iodide. Scale bar: 40uM.

The day after printing (day 1), cell viability was assessed. These had been kept overnight at 37˚C, with at least one change of culture media. Representative images of the constructs are shown in Figure 3.4. Despite some visible differences between the HA-Gel 4% constructs printed with 20G and 22G, where the latter shows a slightly increased number of dead cells, there is not an obvious difference between both types of nozzles when using the HA-Gel 5%. The overall viability of both day 0 and day 1 is represented in Figure 3.5. There is a significant difference (P-value = 0.0006) between using HA-Gel 4% and HA-Gel 5%, considering both nozzle gauge conditions and time-points. We do not observe a major difference using either nozzle gauge within the same bioink, although the non-significant difference could still be somewhat attributed to the light difference of pressures applied, or minor shear-stress caused by the thinner nozzle. However, our results lead us to the conclusion that nozzle gauge is not a critical factor for the viability of HepG2 in bioinks of this composition.

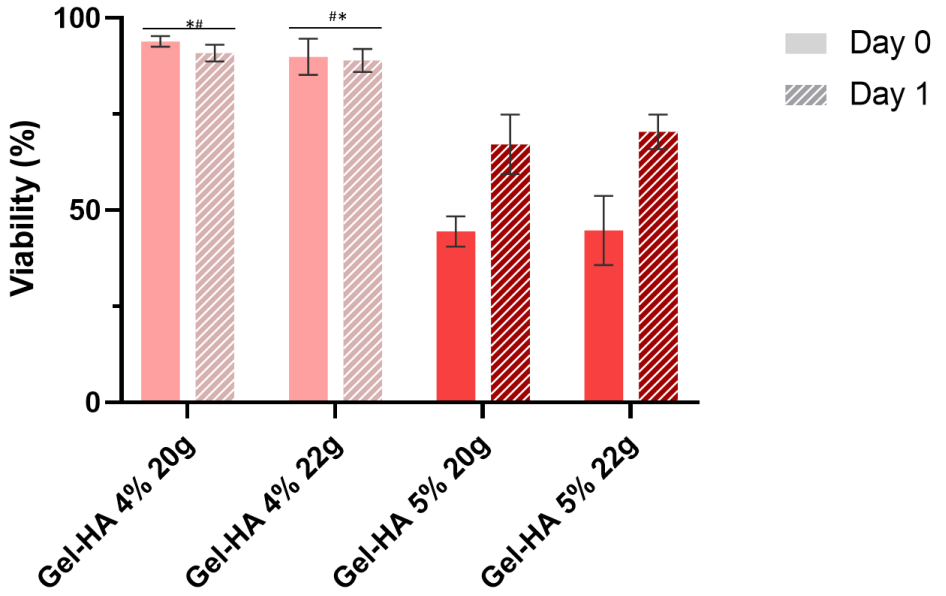

Figure 3.5. Post-printing (day 0) and day 1 viability of HepG2 cells. Nozzle gauge 22G or 20G and HA-Gel 4% or HA-Gel 5%. P-values *< 0.05 compared to GelHA 5% 22G, # < 0.05 compared to compared to GelHA 5% 20G. (Two-way ANOVA, Prism 8).

Nevertheless, it is worth noting that 20G constructs for both bioinks showed better integrity in appearance (Figure 3.6), since thicker filaments extruded yield an overall thicker construct that seemed to hold its structure better than 22G thin filaments. This minor issue might however be corrected by finer tuning of printing speed and design applied.

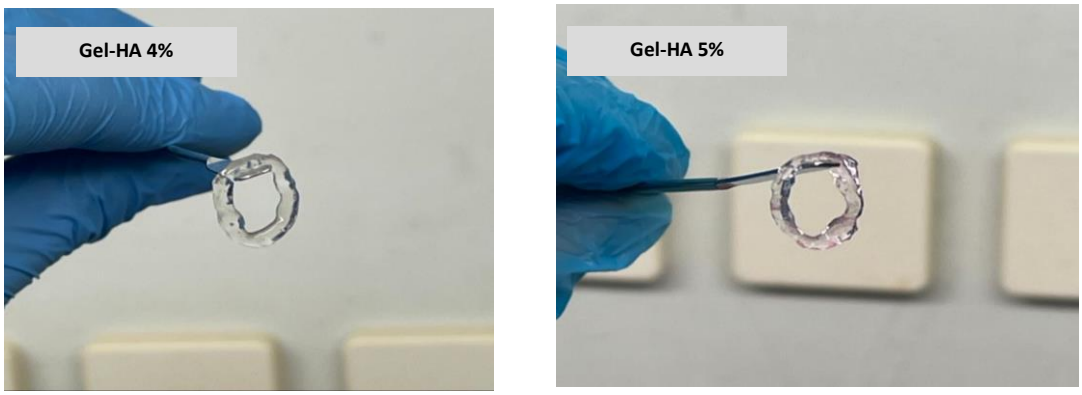

Figure 3.6. Printed cell-laden cylinders after swelling. 20G constructs after 24h incubated in HepG2 culture media at 37˚C. The constructs maintain its structural integrity and can be manipulated.

3.5 Bioinks miscibility evaluation

Ultimately, for bioprinting of organ-like structures several cell-types might be considered, and their microenvironment might differ in composition and mechanical properties, favoring differentiation and proliferation of certain types of cells. For compartmented tissues such as liver lobules, one might be interested in reproducing the complex arrangement of the portal triad around the hepatocyte plates layered with Kupffer and endothelial cells, and a central vein. Using several different bioinks that perform optimally during the printing process as well as have distinct properties to host cells is thus an important achievement in the development of bioprinting strategies for complex tissues.

Several approaches to dye distinct bioinks and evaluate its printability have been used, with fluorescent beads (Colosi et al., 2016), regular food coloring (Webb & Doyle, 2017) , or by fluorescent marking of the cells (Kang et al., 2018). In this study, we evaluated the feasibility of two concentric circles design for cell co-culture, using HA-Gel 4% and HA-Gel 5% for inner and outer circle, respectively. Both HA-Gel bioinks were evaluated since both showed good printability, while gelatin provides cell-adhesion sites lacking in pure HA bioinks. We aimed to determine which gap between the circles should be taken into consideration during the design of the constructs, since we had already observed that strand thickness varied from the theoretical design strand. Therefore, considering a gap between the circles could allow the printing of two distinct structures that did not crosslink between them, but were in close contact to still allow cell interactions. Swelling of the constructs is expected to happen, since after bioprinting, the constructs are covered in cell culture media to provide the necessary nutrients for the encapsulated cells. Hence, we could hypothesize that constructs with a noticeable gap among them post-printing, could be in close contact after incubation in culture media and swelling of the hydrogel networks. Additionally, having two separate structures could be useful to further characterize cell response in each circle individually.

We printed several designs for concentric circles, varying the gap among them. The gap was proportional to the strand thickness (0.59 mm). In Figure 2.5 (see Materials and Methods), the three designs tested are illustrated. We labeled the outer and inner circles with red and green fluorescent dyes (Invitrogen ThermoFischer) respectively, and observed the apparent overlap between the two circles under confocal microscope (Leica Microsystems). In Figure 3.7, representative images of the constructs are shown, post-printing (left) and after incubation in F12 culture media. The aggregates observed for the red dye could be avoided by a short centrifuge spin in the dye solution before mixing with the bioinks.

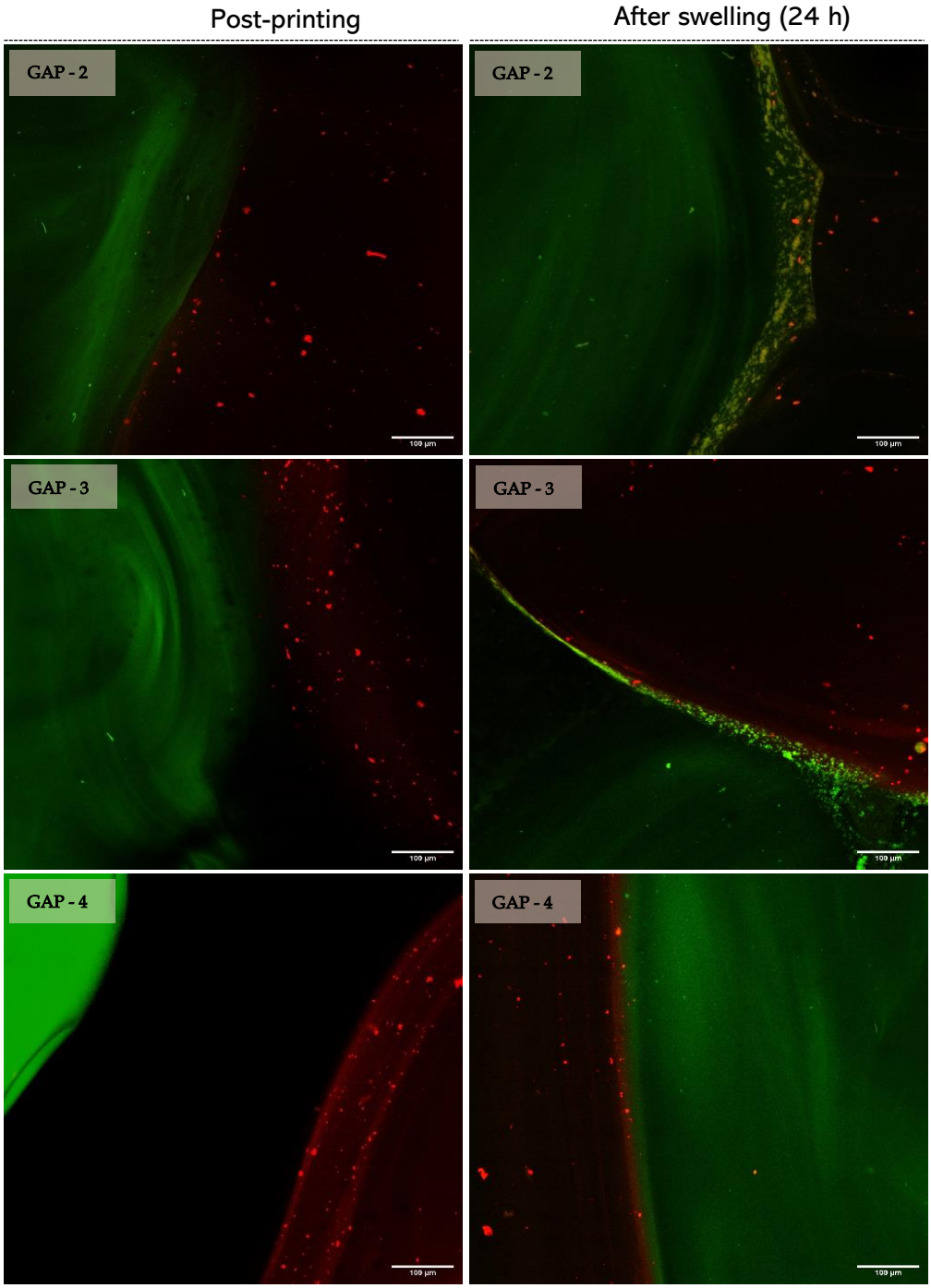

Figure 3.7. Representative images of miscibility. Post-printing miscibility (left) and after 24 h swelling in F12 culture media (right) of printed concentric circles with strand gap proportional to strand thickness (0.59 mm). Green fluorophore was mixed within Gel-HA 4% and red in Gel-HA 5%. Images produced from stacks along Z axis. Left and right images do not correspond to the same point in the constructs.

From the constructs printed with a Gap-2, we can observe that after printing the two rings are in direct contact with no apparent overlap. After swelling, the two rings show an area at the interface where overlapping of the two layers occurs. Despite swelling, if the two rings are overlapping they should be detachable since the crosslinking process was completed post-printing. Nevertheless, it was not possible to physically separate the two without partially tearing apart the structure, since some overlapping had certainly occurred, and the rings had crosslinked in some sections.

As for the Gap-3 constructs, we can notice a slight contact between the rings in the post-printing, while getting full contact after swelling, not seemingly overlapping. The increased concentration of fluorophore at the edge of the rings might result from displacement of the dye molecules by the cell culture swelling the network. Gap-4 constructs show an obvious space between the rings after printing, guaranteeing that the two constructs will crosslink independently. After swelling, the two rings are in close contact without overlapping at the interface. Thus, when two adjacent yet independent constructs are to be printed, we should consider a gap between them of at least three-fold the filament width, taking into account that the printed width will unlikely match the width in the design.

We considered these results as the basis for a promising design for co-culture where a compartmentalized model is desired and close communication at the interface, even diffusion or migration among layers is expected, yet maintaining the advantage of separate manipulation.

3.6 Future perspectives

Future research is aimed toward the study of a differential response of different cells to our bioinks, sustained functionality, and gene expression patterns, as well as paracrine signaling in co-culture models (e.g., HepG2 and Kupffer cells). Multiple studies have already shown that a combination of innovative printing systems with complex designs for co-culture yields remarkable results for liver models. Most use methacrylate-modified UV-cross-linkable polymers or temperature-sensitive gelling polymers. Kang *et al.* used a modified extrusion system where a customized cartridge with a pattern was loaded in the printhead, allowing the introduction of distinct materials within the cartridge compartments (Kang et al., 2020). This way, they managed to print endothelial and HepG2 cells in collagen-based bioinks in strands with a cross-sectional hexagonal pattern within itself, mimicking the structure of liver lobules. A similar approach was used by the same team (Hong et al., 2021) to print injectable lobule-like spheroids, where the co-axial introduction of oil in the nozzle would generate these structures. Ma *et al.* used DLP-bioprinting with 5% GelMA to encapsulate iPSC-derived hepatic cells,

while a blend (1:1) of methacrylate gelatin (5% w/v) and HA (2% w/v) was used to encapsulate supporting endothelial and mesenchymal cells, embedded within hexagonal patterns mimicking liver lobule microarchitecture. Janani *et al*. combined stem cell-derived hepatocyte-like cells with HUVECs (human umbilical vein endothelial cells) and human hepatic stellate cells into extruded constructs with a lobule-like microarchitecture, using decellularized liver ECM microparticles, silk fibroin, and gelatin blend (Janani et al., 2022). The co-culture performance as a drug-induced liver injury (DILI) model was evaluated with hepatotoxicants screening. Fan *et al*. printed HepG2/C3A with HUVEcs in GelMA extruded as adjacent dots in a lobule-like shape. (Fan et al., 2023)

Ultimately, the obtention of a liver model is expected to serve the deciphering of molecular events upon drug exposure, evaluate hepatotoxic drugs, and provide a simplified, yet complex, *in vitro* platform for drug screening. The tunable stiffness of these hydrogels with the varying HA-Gel ratio could pave the way to several liver diseases that are characterized by distinct stiffening in the native tissue (Bomo et al., 2016; Serras et al., 2021; Ye et al., 2019). RNA extraction from these hydrogels is feasible (Rodríguez Fernández, 2021), and would allow the characterization of gene expression. Playing with the bioprinter configuration (e.g., several printheads, sacrifice material, EMD deposition) and adding further design complexity is yet to be explored. Furthermore, a focus on the inclusion of immune cells (i.e., Kupffer-like cells) would provide a way to mimic and study inflammatory responses through cytokine expression. Furthermore, mechanical properties and stability of the cell-laden constructs overtime is also important. A deep study of HepG2 functionality via albumin secretion and cytochrome CYP3A4 activity (i.e., liver function), or CYP1A1 upon drug exposure, cytoskeleton staining and migration studies, may provide a better understanding on how this three-dimensional model compares to 2D platforms, and how the mimicking architecture approaches the native physiological behavior.

4

CONCLUSIONS

The goal of this master thesis was to develop, characterize and optimize new bioinks for extrusion 3D bioprinting with a controlled enzymatic crosslinking.

The viscosity of a range of tyramine-conjugated hyaluronic acid and gelatin-based bioinks was assessed in order to further evaluate its printability and bioprinting performance. HA-only bioinks showed an increase in its shear-stress behavior with an increase in polymer concentration. HA 3% has the closest behavior to our chosen control ink (Cellink START). The addition of gelatin in HA-Gel (80/20) 4 and 5% reduces the shear-stress viscosity of pure HA bioinks. HA-Gel 4% performs as HA 3%, while HA-Gel 5% has a closer behavior to HA 5%.

All HA bioinks were extrudable except HA 5% (w/v). The minimum pressure required to extrude them increased with the polymer concentration and decreased with the addition of Gel. Accordingly, they showed an improved printing resolution with an increase in concentration of polymer, as reflected by uniformity and pore factor parameters. HA 1% and HA 2% were not suitable to yield good quality grid constructs, with poor overall resolution. HA 4%, HA-Gel 4% and HA-Gel 5% provided the best results for the parameters assessed and have the potential to generate high quality constructs.

HepG2 encapsulated in HA-Gel bioinks showed higher post-printing cell viability in the less concentrated bioink HA-Gel 4%, achieving cell viabilities of ca. 90% for nozzle gauge used, whereas viability in HA-Gel 5% constructs showed half the viability, ca. 45% after printing. One day after printing, viability was maintained in HA-Gel 4% constructs, and improved in Gel-HA5% to ca. 70%. Chang *et al.* attributed a recovery in HepG2 viability up to 24h post-

printing to cell recovery from mechanical cell damage (Chang et al., 2008). We can only hypothesize that the increase in viability might be caused by enhanced proliferation in Gel-HA 5%, but these results should be confirmed with viability evaluation in the longer term. The conclusion of this assessment is that polymer concentration has a more significant effect in the cell viability of the printed cells, likely attributed to the shear-stress of higher viscosity inks, rather than caused by narrowing the nozzle gauge.

Miscibility evaluation of both gelatin-HA bioinks showed that to have contiguous structures that do not have overlapping crosslinking but are in contact after printing, a gap of at least 3 times the filament thickness is necessary. Leaving a Gap-4 allows the printing of completely independent structures that can be in contact after swelling.

Overall, these results pave the way for further experiments to evaluate long-term viability of HepG2 cells within these hydrogels, print more complex structures with previous knowledge of the printing parameters required, and introduce other cell types to evaluate whether each bioink provides a differential response in cells, allowing the fabrication of a co-culture system for bioprinted in-vitro liver platforms.

REFERENCES

Abbadessa, A., Mouser, V. H. M., Blokzijl, M. M., Gawlitta, D., Dhert, W. J. A., Hennink, W. E., Malda, J., & Vermonden, T. (2016). A Synthetic Thermosensitive Hydrogel for Cartilage Bioprinting and Its Biofunctionalization with Polysaccharides. *Biomacromolecules*, *17*(6), 2137–2147. https://doi.org/10.1021/acs.biomac.6b00366

Adhikari, J., Roy, A., Das, A., Ghosh, M., Thomas, S., Sinha, A., Kim, J., & Saha, P. (2021). Effects of Processing Parameters of 3D Bioprinting on the Cellular Activity of Bioinks. *Macromolecular Bioscience*, *21*(1), e2000179. https://doi.org/10.1002/mabi.202000179

Arai, K., Yoshida, T., Okabe, M., Goto, M., Mir, T. A., Soko, C., Tsukamoto, Y., Akaike, T., Nikaido, T., Zhou, K., & Nakamura, M. (2017). Fabrication of 3D-culture platform with sandwich architecture for preserving liver-specific functions of hepatocytes using 3D bioprinter. *Journal of Biomedical Materials Research Part A*, *105*(6), 1583–1592. https://doi.org/https://doi.org/10.1002/jbm.a.35905

Asim, S., Tabish, T. A., Liaqat, U., Ozbolat, I. T., & Rizwan, M. (2023). Advances in Gelatin Bioinks to Optimize Bioprinted Cell Functions. *Advanced Healthcare Materials*, *12*(17), 2203148. https://doi.org/https://doi.org/10.1002/adhm.202203148

Bae, J. W., Choi, J. H., Lee, Y., & Park, K. D. (2015). Horseradish peroxidase-catalysed in situ-forming hydrogels for tissue-engineering applications. *Journal of Tissue Engineering and Regenerative Medicine*, *9*(11), 1225–1232. https://doi.org/https://doi.org/10.1002/term.1917

Billiet, T., Gevaert, E., De Schryver, T., Cornelissen, M., & Dubruel, P. (2014). The 3D printing of gelatin methacrylamide cell-laden tissue-engineered constructs with high cell viability. *Biomaterials*, *35*(1), 49–62. https://doi.org/https://doi.org/10.1016/j.biomaterials.2013.09.078

Blaeser, A., Duarte Campos, D. F., Puster, U., Richtering, W., Stevens, M. M., & Fischer, H. (2016). Controlling Shear Stress in 3D Bioprinting is a Key Factor to Balance Printing Resolution and Stem Cell Integrity. *Advanced Healthcare Materials*, *5*(3), 326–333. https://doi.org/https://doi.org/10.1002/adhm.201500677

Bomo, J., Ezan, F., Tiaho, F., Bellamri, M., Langouët, S., Theret, N., & Baffet, G. (2016). Increasing 3D Matrix Rigidity Strengthens Proliferation and Spheroid Development of

Human Liver Cells in a Constant Growth Factor Environment. *Journal of Cellular Biochemistry*, *117*(3), 708–720. https://doi.org/https://doi.org/10.1002/jcb.25356

Bonatti, A. F., Chiesa, I., Vozzi, G., & De Maria, C. (2021). Open-source CAD-CAM simulator of the extrusion-based bioprinting process. *Bioprinting*, *24*, e00172. https://doi.org/https://doi.org/10.1016/j.bprint.2021.e00172

Boularaoui, S., Al Hussein, G., Khan, K. A., Christoforou, N., & Stefanini, C. (2020). An overview of extrusion-based bioprinting with a focus on induced shear stress and its effect on cell viability. *Bioprinting*, *20*, e00093. https://doi.org/https://doi.org/10.1016/j.bprint.2020.e00093

Burdick, J. A., & Prestwich, G. D. (2011). Hyaluronic acid hydrogels for biomedical applications. *Advanced Materials (Deerfield Beach, Fla.)*, *23*(12), H41-56. https://doi.org/10.1002/adma.201003963

Chang, R., Nam, J., & Sun, W. (2008). Effects of Dispensing Pressure and Nozzle Diameter on Cell Survival from Solid Freeform Fabrication–Based Direct Cell Writing. *Tissue Engineering Part A*, *14*(1), 41–48. https://doi.org/10.1089/ten.a.2007.0004

Chliara, M. A., Elezoglou, S., & Zergioti, I. (2022). Bioprinting on Organ-on-Chip: Development and Applications. In *Biosensors* (Vol. 12, Issue 12). https://doi.org/10.3390/bios12121135

Colosi, C., Shin, S. R., Manoharan, V., Massa, S., Costantini, M., Barbetta, A., Dokmeci, M. R., Dentini, M., & Khademhosseini, A. (2016). Microfluidic Bioprinting of Heterogeneous 3D Tissue Constructs Using Low-Viscosity Bioink. *Advanced Materials*, *28*(4), 677–684. https://doi.org/https://doi.org/10.1002/adma.201503310

Cui, X., Breitenkamp, K., Finn, M. G., Lotz, M., & D'Lima, D. D. (2012). Direct human cartilage repair using three-dimensional bioprinting technology. *Tissue Engineering. Part A*, *18*(11–12), 1304–1312. https://doi.org/10.1089/ten.TEA.2011.0543

Dai, X., Ma, C., Lan, Q., & Xu, T. (2016). 3D bioprinted glioma stem cells for brain tumor model and applications of drug susceptibility. *Biofabrication*, *8*(4), 45005. https://doi.org/10.1088/1758-5090/8/4/045005

Darr, A., & Calabro, A. (2009). Synthesis and characterization of tyramine-based hyaluronan hydrogels. *Journal of Materials Science: Materials in Medicine*, *20*(1), 33–44. https://doi.org/10.1007/s10856-008-3540-0

Datta, P., Dey, M., Ataie, Z., Unutmaz, D., & Ozbolat, I. T. (2020). 3D bioprinting for reconstituting the cancer microenvironment. *Npj Precision Oncology*, *4*(1), 18. https://doi.org/10.1038/s41698-020-0121-2

Dávila, J. L., Manzini, B. M., Lopes da Fonsêca, J. H., Mancilla Corzo, I. J., Neto, P. I., Aparecida de Lima Montalvão, S., Annichino-Bizzacchi, J. M., Akira d'Ávila, M., & Lopes da Silva, J. V. (2022). A parameterized g-code compiler for scaffolds 3D bioprinting. *Bioprinting*, *27*, e00222. https://doi.org/https://doi.org/10.1016/j.bprint.2022.e00222

Fan, Z., Wei, X., Chen, K., Wang, L., & Xu, M. (2023). 3D Bioprinting of an Endothelialized Liver Lobule-like Construct as a Tumor-Scale Drug Screening Platform. In *Micromachines* (Vol. 14, Issue 4). https://doi.org/10.3390/mi14040878

Farrance, I., & Frenkel, R. (2012). Uncertainty of Measurement: A Review of the Rules for

Calculating Uncertainty Components through Functional Relationships. *The Clinical Biochemist. Reviews*, *33*(2), 49–75.

Gillispie, G., Prim, P., Copus, J., Fisher, J., Mikos, A. G., Yoo, J. J., Atala, A., & Lee, S. J. (2020). Assessment methodologies for extrusion-based bioink printability. *Biofabrication*, *12*(2), 22003. https://doi.org/10.1088/1758-5090/ab6f0d

Göhl, J., Markstedt, K., Mark, A., Håkansson, K., Gatenholm, P., & Edelvik, F. (2018). Simulations of 3D bioprinting: predicting bioprintability of nanofibrillar inks. *Biofabrication*, *10*(3), 34105. https://doi.org/10.1088/1758-5090/aac872

He, Y., Yang, F., Zhao, H., Gao, Q., Xia, B., & Fu, J. (2016). Research on the printability of hydrogels in 3D bioprinting. *Scientific Reports*, *6*, 29977. https://doi.org/10.1038/srep29977

Henriksson, I., Gatenholm, P., & Hägg, D. A. (2017). Increased lipid accumulation and adipogenic gene expression of adipocytes in 3D bioprinted nanocellulose scaffolds. *Biofabrication*, *9*(1), 15022. https://doi.org/10.1088/1758-5090/aa5c1c

Highley, C. B., Prestwich, G. D., & Burdick, J. A. (2016). Recent advances in hyaluronic acid hydrogels for biomedical applications. *Current Opinion in Biotechnology*, *40*, 35–40. https://doi.org/https://doi.org/10.1016/j.copbio.2016.02.008

Hiller, T., Berg, J., Elomaa, L., Röhrs, V., Ullah, I., Schaar, K., Dietrich, A.-C., Al-Zeer, M. A., Kurtz, A., Hocke, A. C., Hippenstiel, S., Fechner, H., Weinhart, M., & Kurreck, J. (2018). Generation of a 3D Liver Model Comprising Human Extracellular Matrix in an Alginate/Gelatin-Based Bioink by Extrusion Bioprinting for Infection and Transduction Studies. *International Journal of Molecular Sciences*, *19*(10). https://doi.org/10.3390/ijms19103129

Hong, G., Kim, J., Oh, H., Yun, S., Kim, C. M., Jeong, Y.-M., Yun, W.-S., Shim, J.-H., Jang, I., Kim, C.-Y., & Jin, S. (2021). Production of Multiple Cell-Laden Microtissue Spheroids with a Biomimetic Hepatic-Lobule-Like Structure. *Advanced Materials*, *33*(36), 2102624. https://doi.org/https://doi.org/10.1002/adma.202102624

Hwang, C. M., Sant, S., Masaeli, M., Kachouie, N. N., Zamanian, B., Lee, S.-H., & Khademhosseini, A. (2010). Fabrication of three-dimensional porous cell-laden hydrogel for tissue engineering. *Biofabrication*, *2*(3), 35003. https://doi.org/10.1088/1758-5082/2/3/035003

Immohr, M. B., Dos Santos Adrego, F., Teichert, H. L., Schmidt, V., Sugimura, Y., Bauer, S., Barth, M., Lichtenberg, A., & Akhyari, P. (2023). 3D-bioprinting of aortic valve interstitial cells: impact of hydrogel and printing parameters on cell viability. *Biomedical Materials*, *18*(1), 15004. https://doi.org/10.1088/1748-605X/ac9f91

Janani, G., Priya, S., Dey, S., & Mandal, B. B. (2022). Mimicking Native Liver Lobule Microarchitecture In Vitro with Parenchymal and Non-parenchymal Cells Using 3D Bioprinting for Drug Toxicity and Drug Screening Applications. *ACS Applied Materials & Interfaces*, *14*(8), 10167–10186. https://doi.org/10.1021/acsami.2c00312

Jungst, T., Smolan, W., Schacht, K., Scheibel, T., & Groll, J. (2016). Strategies and Molecular Design Criteria for 3D Printable Hydrogels. *Chemical Reviews*, *116*(3), 1496–1539. https://doi.org/10.1021/acs.chemrev.5b00303

Kang, D., Ahn, G., Kim, D., Kang, H.-W., Yun, S., Yun, W.-S., Shim, J.-H., & Jin, S. (2018). Pre-set extrusion bioprinting for multiscale heterogeneous tissue structure fabrication. *Biofabrication*, *10*(3), 35008. https://doi.org/10.1088/1758-5090/aac70b

Kang, D., Hong, G., An, S., Jang, I., Yun, W.-S., Shim, J.-H., & Jin, S. (2020). Bioprinting of Multiscaled Hepatic Lobules within a Highly Vascularized Construct. *Small*, *16*(13), 1905505. https://doi.org/https://doi.org/10.1002/smll.201905505

Kesti, M., Müller, M., Becher, J., Schnabelrauch, M., D'Este, M., Eglin, D., & Zenobi-Wong, M. (2015). A versatile bioink for three-dimensional printing of cellular scaffolds based on thermally and photo-triggered tandem gelation. *Acta Biomaterialia*, *11*, 162–172. https://doi.org/10.1016/j.actbio.2014.09.033

Kobayashi, Y., Okamoto, A., & Nishinari, K. (1994). Viscoelasticity of hyaluronic acid with different molecular weights. *Biorheology*, *31*, 235–244. https://doi.org/10.3233/BIR-1994-31302

Koch, F., Tröndle, K., Finkenzeller, G., Zengerle, R., Zimmermann, S., & Koltay, P. (2020). Generic method of printing window adjustment for extrusion-based 3D-bioprinting to maintain high viability of mesenchymal stem cells in an alginate-gelatin hydrogel. *Bioprinting*, *20*, e00094. https://doi.org/https://doi.org/10.1016/j.bprint.2020.e00094

Kufelt, O., El-Tamer, A., Sehring, C., Schlie-Wolter, S., & Chichkov, B. N. (2014). Hyaluronic Acid Based Materials for Scaffolding via Two-Photon Polymerization. *Biomacromolecules*, *15*(2), 650–659. https://doi.org/10.1021/bm401712q

Kyle, S., Jessop, Z. M., Al-Sabah, A., & Whitaker, I. S. (2017). 'Printability'' of Candidate Biomaterials for Extrusion Based 3D Printing: State-of-the-Art.' *Advanced Healthcare Materials*, *6*(16), 1700264. https://doi.org/https://doi.org/10.1002/adhm.201700264

Lazaridou, M., Bikiaris, D. N., & Lamprou, D. A. (2022). 3D Bioprinted Chitosan-Based Hydrogel Scaffolds in Tissue Engineering and Localised Drug Delivery. In *Pharmaceutics* (Vol. 14, Issue 9). https://doi.org/10.3390/pharmaceutics14091978

Lee, J., Lee, S.-H., Kim, B. S., Cho, Y.-S., & Park, Y. (2018). Development and Evaluation of Hyaluronic Acid-Based Hybrid Bioink for Tissue Regeneration. *Tissue Engineering and Regenerative Medicine*, *15*(6), 761–769. https://doi.org/10.1007/s13770-018-0144-8

Li, X., Liu, B., Pei, B., Chen, J., Zhou, D., Peng, J., Zhang, X., Jia, W., & Xu, T. (2020). Inkjet Bioprinting of Biomaterials. *Chemical Reviews*, *120*(19), 10793–10833. https://doi.org/10.1021/acs.chemrev.0c00008

Liu, S., Wang, T., Li, S., & Wang, X. (2022). Application Status of Sacrificial Biomaterials in 3D Bioprinting. In *Polymers* (Vol. 14, Issue 11). https://doi.org/10.3390/polym14112182

Liu, W., Heinrich, M. A., Zhou, Y., Akpek, A., Hu, N., Liu, X., Guan, X., Zhong, Z., Jin, X., Khademhosseini, A., & Zhang, Y. S. (2017). Extrusion Bioprinting of Shear-Thinning Gelatin Methacryloyl Bioinks. *Advanced Healthcare Materials*, *6*(12), 1601451. https://doi.org/https://doi.org/10.1002/adhm.201601451

Ma, X., Qu, X., Zhu, W., Li, Y.-S., Yuan, S., Zhang, H., Liu, J., Wang, P., Lai, C. S. E., Zanella, F., Feng, G.-S., Sheikh, F., Chien, S., & Chen, S. (2016). Deterministically patterned biomimetic human iPSC-derived hepatic model via rapid 3D bioprinting. *Proceedings of the National Academy of Sciences*, *113*(8), 2206–2211.

https://doi.org/10.1073/pnas.1524510113

Malekpour, A., & Chen, X. (2022). Printability and Cell Viability in Extrusion-Based Bioprinting from Experimental, Computational, and Machine Learning Views. In *Journal of Functional Biomaterials* (Vol. 13, Issue 2). https://doi.org/10.3390/jfb13020040

Mazaki, T., Shiozaki, Y., Yamane, K., Yoshida, A., Nakamura, M., Yoshida, Y., Zhou, D., Kitajima, T., Tanaka, M., Ito, Y., Ozaki, T., & Matsukawa, A. (2014). A novel, visible light-induced, rapidly cross-linkable gelatin scaffold for osteochondral tissue engineering. *Scientific Reports*, *4*, 4457. https://doi.org/10.1038/srep04457

Morata Martínez, M. (2021). Fabrication of 3D printed Gelatin-Hyaluronic Acid hydrogels based on enzyme-mediated tyramine conjugates and other derivatives. *University of Glasgow*, *MRes thesi*.

Mörö, A., Samanta, S., Honkamäki, L., Rangasami, V. K., Puistola, P., Kauppila, M., Narkilahti, S., Miettinen, S., Oommen, O., & Skottman, H. (2023). Hyaluronic acid based next generation bioink for 3D bioprinting of human stem cell derived corneal stromal model with innervation. *Biofabrication*, *15*(1), 15020. https://doi.org/10.1088/1758-5090/acab34

Moroni, L., Boland, T., Burdick, J. A., De Maria, C., Derby, B., Forgacs, G., Groll, J., Li, Q., Malda, J., Mironov, V. A., Mota, C., Nakamura, M., Shu, W., Takeuchi, S., Woodfield, T. B. F., Xu, T., Yoo, J. J., & Vozzi, G. (2018). Biofabrication: A Guide to Technology and Terminology. *Trends in Biotechnology*, *36*(4), 384–402. https://doi.org/https://doi.org/10.1016/j.tibtech.2017.10.015

Moya, A., Ortega-Ribera, M., Guimerà, X., Sowade, E., Zea, M., Illa, X., Ramon, E., Villa, R., Gracia-Sancho, J., & Gabriel, G. (2018). Online oxygen monitoring using integrated inkjet-printed sensors in a liver-on-a-chip system. *Lab on a Chip*, *18*(14), 2023–2035. https://doi.org/10.1039/c8lc00456k

Murphy, S. V, & Atala, A. (2014). 3D bioprinting of tissues and organs. *Nature Biotechnology*, *32*(8), 773–785. https://doi.org/10.1038/nbt.2958

Naghieh, S., & Chen, X. (2021). Printability–A key issue in extrusion-based bioprinting. *Journal of Pharmaceutical Analysis*, *11*(5), 564–579. https://doi.org/https://doi.org/10.1016/j.jpha.2021.02.001

Nair, K., Gandhi, M., Khalil, S., Yan, K. C., Marcolongo, M., Barbee, K., & Sun, W. (2009). Characterization of cell viability during bioprinting processes. *Biotechnology Journal*, *4*(8), 1168–1177. https://doi.org/https://doi.org/10.1002/biot.200900004

Naranjo-Alcazar, R., Bendix, S., Groth, T., & Gallego Ferrer, G. (2023). Research Progress in Enzymatically Cross-Linked Hydrogels as Injectable Systems for Bioprinting and Tissue Engineering. In *Gels* (Vol. 9, Issue 3). https://doi.org/10.3390/gels9030230

Nazir, A., Gokcekaya, O., Md Masum Billah, K., Ertugrul, O., Jiang, J., Sun, J., & Hussain, S. (2023). Multi-material additive manufacturing: A systematic review of design, properties, applications, challenges, and 3D printing of materials and cellular metamaterials. *Materials & Design*, *226*, 111661. https://doi.org/https://doi.org/10.1016/j.matdes.2023.111661

Ning, L., Betancourt, N., Schreyer, D. J., & Chen, X. (2018). Characterization of Cell Damage

and Proliferative Ability during and after Bioprinting. *ACS Biomaterials Science & Engineering*, *4*(11), 3906–3918. https://doi.org/10.1021/acsbiomaterials.8b00714

Ouyang, L., Highley, C. B., Rodell, C. B., Sun, W., & Burdick, J. A. (2016). 3D Printing of Shear-Thinning Hyaluronic Acid Hydrogels with Secondary Cross-Linking. *ACS Biomaterials Science & Engineering*, *2*(10), 1743–1751. https://doi.org/10.1021/acsbiomaterials.6b00158

Parsa, S., Gupta, M., Loizeau, F., & Cheung, K. C. (2010). Effects of surfactant and gentle agitation on inkjet dispensing of living cells. *Biofabrication*, *2*(2), 25003. https://doi.org/10.1088/1758-5082/2/2/025003

Paxton, N., Smolan, W., Böck, T., Melchels, F., Groll, J., & Jungst, T. (2017). Proposal to assess printability of bioinks for extrusion-based bioprinting and evaluation of rheological properties governing bioprintability. *Biofabrication*, *9*(4), 44107. https://doi.org/10.1088/1758-5090/aa8dd8

Petta, D., Grijpma, D. W., Alini, M., Eglin, D., & D'Este, M. (2018). Three-Dimensional Printing of a Tyramine Hyaluronan Derivative with Double Gelation Mechanism for Independent Tuning of Shear Thinning and Postprinting Curing. *ACS Biomaterials Science & Engineering*, *4*(8), 3088–3098. https://doi.org/10.1021/acsbiomaterials.8b00416

Potere, F., Belgio, B., Croci, G. A., Tabano, S., Petrini, P., Dubini, G., Boschetti, F., & Mantero, S. (2022). 3D bioprinting of multi-layered segments of a vessel-like structure with ECM and novel derived bioink . In *Frontiers in Bioengineering and Biotechnology* (Vol. 10). https://www.frontiersin.org/articles/10.3389/fbioe.2022.918690

Poveda-Reyes, S., Moulisova, V., Sanmartín-Masiá, E., Quintanilla-Sierra, L., Salmerón-Sánchez, M., & Ferrer, G. G. (2016). Gelatin—Hyaluronic Acid Hydrogels with Tuned Stiffness to Counterbalance Cellular Forces and Promote Cell Differentiation. *Macromolecular Bioscience*, *16*(9), 1311–1324. https://doi.org/https://doi.org/10.1002/mabi.201500469

Rayahin, J. E., Buhrman, J. S., Zhang, Y., Koh, T. J., & Gemeinhart, R. A. (2015). High and Low Molecular Weight Hyaluronic Acid Differentially Influence Macrophage Activation. *ACS Biomaterials Science & Engineering*, *1*(7), 481–493. https://doi.org/10.1021/acsbiomaterials.5b00181

Ribeiro, A., Blokzijl, M. M., Levato, R., Visser, C. W., Castilho, M., Hennink, W. E., Vermonden, T., & Malda, J. (2018). Assessing bioink shape fidelity to aid material development in 3D bioprinting. *Biofabrication*, *10*(1), 14102. https://doi.org/10.1088/1758-5090/aa90e2

Rodríguez Fernández, J. (2021). *Desarrollo de hidrogeles biomiméticos inyectables para cultivo celular hepático.* https://doi.org/http://hdl.handle.net/10251/160535

Rutz, A. L., Hyland, K. E., Jakus, A. E., Burghardt, W. R., & Shah, R. N. (2015). A multimaterial bioink method for 3D printing tunable, cell-compatible hydrogels. *Advanced Materials (Deerfield Beach, Fla.)*, *27*(9), 1607–1614. https://doi.org/10.1002/adma.201405076

Sakai, S., Harada, R., & Kotani, T. (2021). Freeform 3D Bioprinting Involving Ink Gelation by Cascade Reaction of Oxidase and Peroxidase: A Feasibility Study Using Hyaluronic Acid-Based Ink. In *Biomolecules* (Vol. 11, Issue 12). https://doi.org/10.3390/biom11121908

Sakai, S., Hirose, K., Taguchi, K., Ogushi, Y., & Kawakami, K. (2009). An injectable, in situ

enzymatically gellable, gelatin derivative for drug delivery and tissue engineering. *Biomaterials*, *30*(20), 3371–3377. https://doi.org/10.1016/j.biomaterials.2009.03.030

Sanmartín-Masiá, E., Poveda-Reyes, S., & Gallego Ferrer, G. (2017). Extracellular matrix–inspired gelatin/hyaluronic acid injectable hydrogels. *International Journal of Polymeric Materials and Polymeric Biomaterials*, *66*(6), 280–288. https://doi.org/10.1080/00914037.2016.1201828

Sarker, M., Izadifar, M., Schreyer, D., & Chen, X. (2018). Influence of ionic crosslinkers (Ca2+/Ba2+/Zn2+) on the mechanical and biological properties of 3D Bioplotted Hydrogel Scaffolds. *Journal of Biomaterials Science, Polymer Edition*, *29*(10), 1126–1154. https://doi.org/10.1080/09205063.2018.1433420

Schwab, A., Levato, R., D'Este, M., Piluso, S., Eglin, D., & Malda, J. (2020). Printability and Shape Fidelity of Bioinks in 3D Bioprinting. *Chemical Reviews*, *120*(19), 11028–11055. https://doi.org/10.1021/acs.chemrev.0c00084

Serras, A. S., Rodrigues, J. S., Cipriano, M., Rodrigues, A. V, Oliveira, N. G., & Miranda, J. P. (2021). A Critical Perspective on 3D Liver Models for Drug Metabolism and Toxicology Studies . In *Frontiers in Cell and Developmental Biology* (Vol. 9). https://www.frontiersin.org/articles/10.3389/fcell.2021.626805

Skardal, A., Zhang, J., McCoard, L., Xu, X., Oottamasathien, S., & Prestwich, G. D. (2010). Photocrosslinkable hyaluronan-gelatin hydrogels for two-step bioprinting. *Tissue Engineering. Part A*, *16*(8), 2675–2685. https://doi.org/10.1089/ten.TEA.2009.0798

Sun, L., Yang, H., Wang, Y., Zhang, X., Jin, B., Xie, F., Jin, Y., Pang, Y., Zhao, H., Lu, X., Sang, X., Zhang, H., Lin, F., Sun, W., Huang, P., & Mao, Y. (2020). Application of a 3D Bioprinted Hepatocellular Carcinoma Cell Model in Antitumor Drug Research . In *Frontiers in Oncology* (Vol. 10). https://www.frontiersin.org/articles/10.3389/fonc.2020.00878

Tang, D., Tare, R. S., Yang, L.-Y., Williams, D. F., Ou, K.-L., & Oreffo, R. O. C. (2016). Biofabrication of bone tissue: approaches, challenges and translation for bone regeneration. *Biomaterials*, *83*, 363–382. https://doi.org/https://doi.org/10.1016/j.biomaterials.2016.01.024

Tavianatou, A. G., Caon, I., Franchi, M., Piperigkou, Z., Galesso, D., & Karamanos, N. K. (2019). Hyaluronan: molecular size-dependent signaling and biological functions in inflammation and cancer. *The FEBS Journal*, *286*(15), 2883–2908. https://doi.org/https://doi.org/10.1111/febs.14777

Taymour, R., Chicaiza-Cabezas, N. A., Gelinsky, M., & Lode, A. (2022). Core–shell bioprinting of vascularized in vitro liver sinusoid models. *Biofabrication*, *14*(4), 45019. https://doi.org/10.1088/1758-5090/ac9019

Ulubayram, K., Aksu, E., Gurhan, S. I. D., Serbetci, K., & Hasirci, N. (2002). Cytotoxicity evaluation of gelatin sponges prepared with different cross-linking agents. *Journal of Biomaterials Science, Polymer Edition*, *13*(11), 1203–1219. https://doi.org/10.1163/156856202320892966

Vaca-González, J. J., Clara-Trujillo, S., Guillot-Ferriols, M., Ródenas-Rochina, J., Sanchis, M. J., Ribelles, J. L. G., Garzón-Alvarado, D. A., & Ferrer, G. G. (2020). Effect of electrical stimulation on chondrogenic differentiation of mesenchymal stem cells cultured in

hyaluronic acid – Gelatin injectable hydrogels. *Bioelectrochemistry*, *134*, 107536. https://doi.org/https://doi.org/10.1016/j.bioelechem.2020.107536

Wang, X., Ao, Q., Tian, X., Fan, J., Tong, H., Hou, W., & Bai, S. (2017). Gelatin-Based Hydrogels for Organ 3D Bioprinting. In *Polymers* (Vol. 9, Issue 9). https://doi.org/10.3390/polym9090401

Webb, B., & Doyle, B. J. (2017). Parameter optimization for 3D bioprinting of hydrogels. *Bioprinting*, *8*, 8–12. https://doi.org/https://doi.org/10.1016/j.bprint.2017.09.001

Williams, C. G., Malik, A. N., Kim, T. K., Manson, P. N., & Elisseeff, J. H. (2005). Variable cytocompatibility of six cell lines with photoinitiators used for polymerizing hydrogels and cell encapsulation. *Biomaterials*, *26*(11), 1211–1218. https://doi.org/10.1016/j.biomaterials.2004.04.024

Wüst, S., Godla, M. E., Müller, R., & Hofmann, S. (2014). Tunable hydrogel composite with two-step processing in combination with innovative hardware upgrade for cell-based three-dimensional bioprinting. *Acta Biomaterialia*, *10*(2), 630–640. https://doi.org/10.1016/j.actbio.2013.10.016

Xu, X., Jagota, A., Peng, S., Luo, D., Wu, M., & Hui, C.-Y. (2013). Gravity and Surface Tension Effects on the Shape Change of Soft Materials. *Langmuir*, *29*(27), 8665–8674. https://doi.org/10.1021/la400921h

Ye, S., Boeter, J. W. B., Penning, L. C., Spee, B., & Schneeberger, K. (2019). Hydrogels for Liver Tissue Engineering. *Bioengineering (Basel, Switzerland)*, *6*(3). https://doi.org/10.3390/bioengineering6030059

Zhou, M., Lee, B. H., Tan, Y. J., & Tan, L. P. (2019). Microbial transglutaminase induced controlled crosslinking of gelatin methacryloyl to tailor rheological properties for 3D printing. *Biofabrication*, *11*(2), 25011. https://doi.org/10.1088/1758-5090/ab063f